Interim Progress Report on NASA Grant NAG5-2232

"Receiver Design, Performance Analysis, and Evaluation for Space-Borne Laser Altimeters and Space-to-Space Laser Ranging Systems"

for the period of Oct. 16, 1993 to April 14, 1994

Frederic M. Davidson,
Xiaoli Sun
Christopher T. Field

Department of Electrical and Computer Engineering
The Johns Hopkins University, Baltimore, MD 21218-2686

May 1994

Summary

The following is a list of our accomplishments in the past 12 months. Most of the objectives in our original proposal for this period have been achieved. Additional research was also performed at the request of NASA/GSFC, code 924.

1. Receiver performance study of space-borne laser altimeters and cloud and aerosol lidars:

We have developed a procedure about how to simulate the APD output signal using the much more exact models given by McIntyre and Webb for the APD. The preamplifier noise model was also improved. This APD simulator will be used to update the existing Laser Altimeter Simulator which currently uses an over simplified Gaussian model for the APD output photocurrent. A separate write-up titled "Computer Simulation of the output signal from an APD" is attached.

A computer program was written to simulate the noise counter output of the laser altimeter. The nearly exact models for the APD and preamplifier noise were used. The noise counter output serves as the input to the automatic threshold adjustment circuit of the laser altimeter. This program is currently being incorporated in the Laser Altimeter Simulator, version 4.0. A short report about our program titled "Simulation of the number of threshold crossings due to noise between laser shots for the GLAS simulator" is included in this report.

A computer program was written using the software Mathcad to analytically calculate the performance of APD laser altimeter receivers based on Webb's distribution for the APD output. The Gaussian model was shown to have series shortcomings. The program used the Geoscience Laser Altimeter System (GLAS) as an example. A copy of the program, "GLAS altimeter link margin analysis", is attached.

A simple laser ranging system was set up in the lab. A low power 1.06 μm wavelength laser diode was used as the test laser transmitter. The use of a laser diode allows us to arbitrarily alter the laser pulse shape in order to simulate the altimeter return signals. The total timing

jitter of the pulse generator, the laser, and the counter/timer under strong input signal conditions was found to be about 60 ps, which was well within 300 ps required by GLAS.

We conducted with D. Reusser of USRA a study of radiation damage to Si APDs for the radiation environment similar to that of GLAS. We found that all previous radiation damage tests used either electron or gamma rays as the radiation sources. The radiation of concern for low earth orbit such as GLAS is primarily high energy protons at the so called South Atlantic Anomaly region and poles of the geomagnetosphere. Based on our study, Si APDs were expected to suffer long term radiation damage, which may be negligible for linear mode operation but overwhelming for Geiger mode operation. A proton radiation damage test for silicon APDs was planned.

We also performed a research of available Si APDs as candidates for the GLAS altimeter receiver. A custom APD preamplifier module by EG&G was chosen. Three devices were purchased and they were scheduled for delivery in May 1994.

The receiver signal to noise ratio for the GLAS cloud lidar was calculated assuming a PMT photon counter is used as the photodetector. The total charges drawn from the PMT photocathode and anode were also computed. A copy of the Mathcad program printout, "GLAS cloud lidar receiver photon rate calculation", is included in this progress report.

2. Receiver performance analysis for space-to-space laser ranging systems:

All our work in this area was related to the Gravity And Magnetic Experiment Survey (GAMES) mission proposed by NASA/GSFC, code 924.

We studied different types of receiver structures for GAMES. The most attractive receiver design appeared to be the one used by the National Radio Astronomy Organization (NRAO), which used a down-converter and a narrow band filter instead of a PLL. NRAO had successfully used this type of receiver for laser ranging to stationary

objects. The receiver can be greatly simplified when using this approach as compared to other types of receivers.

We studied the receiver performance for a moving target. The receiver estimation bias due to Doppler shift was analyzed. The effects of the finite sample rate and number of bits of the analog to digital converter were calculated. The results were consistent with the actual measurements. A short report on this subject, "Use of the NRAO method for the GAMES fine ranging receiver", is attached.

The link analysis of the GAMES fine ranging system was improved and included the use of APDs. The effects of the PMT gain and stray light were calculated. The receiver performance using a PMT and an APD was compared. The program was used to calculate the performance of the latest version of the GAMES laser ranging instrument (LRI-2).

The receiver design for a multitone laser ranging system was studied. A copy of our results, "Receiver performance analysis of a multiple tone laser ranging system", is attached.

CCD cameras, star trackers, and quad APDs as the tracking detectors for GAMES were also studied.

We have estimated (with D. Reusser, N. Walsh, and K. Mehalick) the amount of stray light incident on the fine ranging and coarse ranging detectors. The major stray light source was found to be sunlit clouds. The sun glint from the ocean was shown to be negligible. The moon and other planets and stars were found to have little contribution to the total stray light onto the detector unless they are in the telescope field of view. The minimum angle was found between the sun and the telescope line of sight for the receiver to remain operational. The details of this study were already reported in our progress report for the previous six month period.

A preliminary study of radiation damage to the PMT and CCDs for GAMES was completed (with D. Reusser). The major radiation damage to PMTs occurred on the glass window. PMTs have been tested and shown to suffer little performance degradation for the radiation dose experienced

by GAMES. CCDs were found to be relatively sensitive to radiation damage. Test data in the literature showed that regular CCD cameras would suffer serious long term damage if used in GAMES and the resultant performance degradation would not be acceptable. A well designed rad-hard CCD camera, on the other hand, has been shown to suffer negligible long term damage for the radiation dose experienced by GAMES. A separate report, "Space radiation effects on photodetectors for GAMES and GLAS", is attached, which included our results on PMTs, CCDs and Si APDs.

Pseudo noise (PN) code laser ranging systems were studied for the GAMES coarse ranging subsystem. Receiver performance was analyzed for both baseband and subcarrier modulated PN ranging codes. The so called JPL ranging codes were studied as a possible candidate for the GAMES coarse ranging system. The power spectra of regular PN ranging codes and JPL ranging codes were calculated. Included in this report are copies of two short reports, "Receiver performance analysis of the GAMES PN code coarse ranging subsystems" and "Power spectrum of PN ranging codes."

3. Receiver performance study for the Mars Environmental Survey (MESUR):

We have done preliminary estimates of the solar background photon flux. It is expected that most of the detected photons will be of solar origin. The number of bits required to store each histogram bit and the signal to noise ratio both depend strongly on the number of detected signal photons, the solar photon flux, and the averaging time. Therefore specification of the histogram electronics and averaging time depend on an accurate estimate of the solar flux.

We have investigated several low power, radiation tolerant computers. A Zilog Z80 has be selected for prototyping. In addition, a low power memory has been selected.

Different types of quenching circuitry for the Geiger mode APD photon counters were studied and tested for the lowest electrical power consumption.

Computer Simulation of the Signal Output from an APD

Xiaoli Sun
The Johns Hopkins University

1. Introduction

A computer simulator of space borne laser altimeters which use silicon APD has been developed by NASA/GSFC. However, the signal output from the APD was simulated approximately using the Gaussian distribution. The actual distribution of the signal output from an APD was given by McIntyre [1] which was significantly different from the Gaussian distribution, especially at the tails of the probability density functions. A close approximation of the McIntyre distribution has been given by Webb [2]. This report attempts to give a guide line of how to upgrade the existing laser altimeter simulator with the much more exact APD models by McIntyre or Webb.

The signal to be simulated consists of photoelectrons output from the APD and noise from the preamplifier. The former follows the McIntyre distribution and the latter follows the Gaussian distribution. The two are independent of each other. The output of the simulation program consists of discrete samples at a specified sampling rate. Each sample is equal to the signal averaged over the sampling interval. From now on, we define the signal as the input current to the preamplifier. All the noise sources will also be converted to their equivalent noise currents at the input to the preamplifier.

2. Simulation of the Preamplifier Noise

The preamplifier noise follows the Gaussian distribution. Press et al [3] have shown subroutine for generating standard Gaussian random variable. We need only to scale this standard Gaussian random variable, y_{g0}, to obtain the preamplifier noise output, y_g, according to the relationship

$$y_g = \sigma y_{g0} + \mu \tag{1}$$

where μ and σ are the mean and standard deviation. The mean of amplifier noise can be considered to be zero. The variance of preamplifier noise can be calculated as

$$\sigma^2 = \frac{1}{2\pi}\int_0^{\infty} \frac{\sin^2(\omega\Delta\tau/2)}{(\omega\Delta\tau/2)^2} N(\omega)d\omega \tag{2}$$

where $N(\omega)$ is the one sided noise power spectrum of the preamplifier and $\Delta\tau$ is the sampling interval. The first part of the integrand in (2) results from the fact that each sample is the average signal over the sampling interval (integration of the actual signal over $\Delta\tau$ and then divided by $\Delta\tau$). If the preamplifier contains a FET as the front stage, the noise power spectrum can be written as [4]

$$N(\omega) = \frac{4KT_a}{R_f} + 2qI_g + \frac{4KT_a\Gamma}{g_m R_f} + \frac{4KT_a\Gamma}{g_m}(\omega C_i)^2 \tag{10}$$

where K is the Botzmann's constant, T_a(°K) is the ambient temperature, R_f is the transimpedance of the preamplifier, g_m is the transconductance of the FET, Γ is a factor close to unity, and C_i is the total capacitance at the input of the preamplifier.

When the altimeter receiver bandwidth is below 200 MHz, one can often approximate the preamplifier noise as white Gaussian noise with the variance given as

$$\sigma^2 = \frac{4KT_n}{R_f}\frac{1}{2\Delta\tau} \tag{11}$$

where $T_n(°K)$ is the equivalent noise temperature.

3. Simulation of the Photocurrent Output from the APD

The sampled output of an APD can be modeled as a discrete random process which is equal to the number of photoelectrons during the sampling interval times the electron charge and then divided by the sampling interval. The probability of the number of photoelectrons has been shown to follow the so-called McIntyre distribution [1], as

$$P(m|\lambda(t)\Delta\tau) = \sum_{n=1}^{m} P_M(m|n)\cdot\frac{(\lambda(t)\Delta\tau)^n}{n!}e^{-\lambda(t)\Delta\tau}, \qquad m \geq 1$$

$$P(0|\lambda(t)\Delta\tau) = e^{-\lambda(t)\Delta\tau} \tag{12}$$

with $P_M(m|n)$ the probability of generating m secondary photoelectrons in response to n primary photoelectrons, as

$$P_M(m|n) = \frac{n\Gamma\left(\frac{m}{1-k_{eff}}+1\right)}{m(m-n)!\,\Gamma\left(\frac{k_{eff}m}{1-k_{eff}}+1+n\right)} \cdot\left[\frac{1+k_{eff}(G-1)}{G}\right]^{n+\frac{k_{eff}m}{1-k_{eff}}}\cdot\left[\frac{(1-k_{eff})(G-1)}{G}\right]^{m-n} \tag{13}$$

where k_{eff} is the APD hole to electron ionization coefficient ratio, G is the average APD gain, and $\lambda(t)$ is the primary photon counting rate given by

$$\lambda(t) = \frac{\eta}{hf}\left[P_s(t) + P_0\right] + \frac{I_b}{q} \tag{14}$$

where η is the APD quantum efficiency, hf is the photon energy, $P_S(t)$ is the input optical signal power, P_0 is the background radiation power assuming to be constant, I_b is the APD bulk leakage current, and q is the electron charge.

A very close approximation to (12) was given by Webb et al [2] for $\lambda(t)\Delta\tau >> 1$, as

$$P_W(m|\lambda(t)\Delta\tau) \approx \frac{1}{\sqrt{2\pi G^2 F\lambda(t)\Delta\tau}} \cdot \frac{1}{\left[1+\frac{(m-G\lambda(t)\Delta\tau)(F-1)}{GF\lambda(t)\Delta\tau}\right]^{\frac{3}{2}}} \cdot \exp\left[-\frac{(m-G\lambda(t)\Delta\tau)^2}{2G^2F\lambda(t)\Delta\tau\left[1+\frac{(m-G\lambda(t)\Delta\tau)(F-1)}{GF\lambda(t)\Delta\tau}\right]}\right], \quad m > \lambda(t)\Delta\tau \tag{15}$$

where F is the APD excess noise factor which can be calculated as

$$F = k_{eff}G + \left(2 - \frac{1}{G}\right)(1 - k_{eff}). \tag{16}$$

It also known [5] that the Webb's approximation becomes inaccurate as $\lambda(t)\Delta\tau >> 1$. Therefore, it is suggested to use Eq. (15) only for $\lambda(t)\Delta\tau > 10$.

Because the complexity of the probability distributions for the APD, one cannot generate the random variable as an analytical function of

a uniform distributed random variable. Instead, the rejection method described in [3] has to be used. A comparison function has to be found when using the rejection method. The comparison function is a function which is greater than the desired probability distribution function for all possible value of the random variable and the total area under the curve is finite. The inverse function of the indefinite integral of the comparison function should also be known analytically. The area (integral) of the comparison function should also be as small as possible since the time required to generate the random number increases with the area of the comparison function.

We may simulate the APD photoelectron output for $\lambda(t)\Delta\tau \leq 10$ in two steps. First we generate a Poisson variables to simulate the number of primary photo electrons. We then simulate how many secondary photoelectrons each primary photoelectron will generate according to Eq. (13) with n=1. The APD output should be the sum of secondary photoelectrons for all primary photoelectrons. This procedure involves calling a Poisson random number generator once and then calling a McIntyre random number generator n times with n the outcome of the Poisson random number generator. This method only requires a comparison function for the McIntyre distribution for the n=1 case.

The Poisson random number generator can be implemented using the computer subroutine provided by Press et al [3]. The McIntyre random number generator can be realized similarly but with the propitiate probability distribution and comparison functions. We may still use a Lorentzian distribution as the comparison function, i.e.,

$$f(x)=\frac{c_0}{1+\frac{(x-x_0)^2}{a_0^2}} \tag{17}$$

We need to find a set of values for c_0, x_0, and a_0 such that $f(m)>P_M(m|1)$ and $\int_{-\infty}^{\infty} f(x)dx$ as small as possible for all possible values of m. One example is $c_0=4/G$, $x_0=-G/50$, and $a_0=G/3$. Appendix A shows plots of $P_M(m|1)$ and f(x) with the above parameter values for various APD gains from G=50 to 500.

For $\lambda(t)\Delta\tau$ >10, one may simulate the APD output in one step using the Webb's approximation (15) to save computer times. A suggestion for the comparison function is still the same as Eq. (17) but with $c_0=1/2G(F\lambda(t)\Delta\tau)^{1/2}$, $x_0=G\lambda(t)\Delta\tau$, and $a_0=G(2F\lambda(t)\Delta\tau)^{1/2}$. Appendix B shows plots of the Webb's approximation and the suggested comparison function for $\lambda(t)\Delta\tau$ =100 and various values of the average APD gain.

APDs also have surface leakage current which is not multiplied by the APD gain. This part of the APD dark current should be modeled as a DC current with its shot noise contribution following the Gaussian distribution with the mean and variance given by

$$\begin{aligned}\mu &= qI_s\Delta\tau \\ \sigma_s^2 &= qI_s\Delta\tau\end{aligned} \tag{18}$$

where I_s is the surface leakage current. This noise can be added to the total preamplifier noise.

References

[1] R. J. McIntyre, "The distribution of gains in uniformly multiplying avalanche photodiodes: Theory," *IEEE Trans. Electron Devices*, vol. ED-19, pp. 703-713, Sept. 1972.

[2] P. P. Webb, R. J. McIntyre, and J. Conradi, "Properties of avalanche photodiodes," *RCA Review*, vol. 35, pp. 235-278, June 1974.

[3] W. H. Press, Saul A. Teukolsky, W. T. Vetterling, and B. P. Flannery, *Numerical Recipes in Fortran, The art of Scientific Computing*, 2nd ed., Cambridge University Press, New York, 1992.

[4] R. G. Smith and S. D. Personick, "Receiver design for optical fiber communication systems," in , Spring-Verlag, New York, 1980, ch. 4.

[5] F. M. Davidson and X. Sun, "Gaussian approximation versus nearly exact performance analysis of optical communication systems with PPM signaling and APD receivers," *IEEE Trans. Commun.*, vol. COM-36, no. 11, pp. 1185-1192, Nov. 1988.

Simulation of the Number of Threshold Crossings due to Noise between Laser Shots for the GLAS Simulator

Xiaoli Sun
The Johns Hopkins University
January 1994

1. Theory

The threshold crossings due to noise, or false alarms, can be assumed to follow the Poisson distribution for a reasonably low false alarm probability. The rate of false alarms can be calculated as [1]

$$T_{FA}^{-1}=\frac{p_{fa}}{\tau} \tag{1}$$

where p_{fa} is the probability of threshold crossing at a fixed time within the observation interval due to noise alone and τ is the average pulsewidth of the false alarms, which is roughly equal to the reciprocal of the receiver bandwidth. The total number of false alarms in an observation time interval, T, can be written as

$$P_{FA}(n)=\frac{(N_{FA})^n}{n!}\exp(-N_{FA}). \tag{2}$$

where N_{FA} is the average number of false alarms given as

$$N_{FA}=\frac{T}{T_{FA}}=\frac{T}{\tau}p_{fa} \tag{3}$$

The point false alarm probability, p_{fa}, can be calculated as

$$p_{fa}=\int_{x_T}^{\infty} p(x|0)dx \tag{4}$$

with $p(x|0)$ the probability density function (p.d.f.) when no signal is transmitted. For convenience, we define the random variable x as the

equivalent number of photoelectrons integrated over τ second in front of the preamplifier.

There are two independent noise sources, the APD dark noise and the preamplifier noise. The p.d.f. of the total noise is given as the convolution of the p.d.f. of the two noise sources.

The number of equivalent dark photoelectrons from the APD has been shown to follow the McIntyre-Conradi distribution [2][3], which is rather complicated. A much simpler and yet very close approximation to the McIntyre-Conradi distribution has been given by Webb et al. [4], as

$$P_{PD}(x|\mu_0)=\frac{1}{\sqrt{2\pi G^2 F\mu_0}}\frac{1}{\left[1+\frac{(x-G\mu_0)(F-1)}{GF\mu_0}\right]^{3/2}}\exp\left\{\frac{-(x-G\mu_0)^2}{2G^2F\mu_0\left[1+\frac{(x-G\mu_0)(F-1)}{GF\mu_0}\right]}\right\},$$

$$x > \mu_0 \qquad (5)$$

where G is the average APD gain, F is the APD excess noise factor, and μ_0 is the average number of equivalent primary APD dark photoelectrons given as

$$\mu_0=\left(n_b+\frac{I_b\tau}{q}\right) \qquad (6)$$

where n_b is the average background radiation noise count over a laser pulse width time, I_b is the APD bulk leakage current, and q is the electron charge. The random variable, x, in (5) should be a discrete number. But the average APD gain is often set to a relatively large value for high receiver sensitivity and the distribution of x may considered as continuous. The APD excess noise factor in (5) can be calculated as [4]

$$F=G\cdot k_{eff}+(2-\frac{1}{G})(1-k_{eff}) \tag{7}$$

where k_{eff} is the APD ionization coefficient ratio of holes and electrons.

The noise contribution from the preamplifier appears additive and follows the Gaussian distribution with zero mean and variance given by [5]

$$\sigma^2=\frac{2KT_n\tau}{R_l q^2}+\frac{I_s\tau}{q} \tag{8}$$

where K is Boatsman constant, $T_n(°K)$ is the equivalent noise temperature of the preamplifier, and R_l is the APD load resistance (the preamplifier gain). We have assumed here that the amplifier noise is white noise, which is a good approximation up to a bandwidth of about 200 MHz. The APD surface leakage current also contribute additive white Gaussian noise and it can be included in the equivalent noise temperature.

The p.d.f. the total noise is the convolution integral of Eq. (5) and the p.d.f. of the Gaussian noise, i.e.,

$$p(x|0)=\int_{\mu_0}^{\infty}\frac{1}{\sqrt{2\pi}\sigma}\exp\left[-\frac{(x-y)^2}{2\sigma^2}\right]P_{PD}(y|\mu_0)dy. \tag{9}$$

The probability of false alarm can be obtained by substituting (5) into (9) and then (4), as

$$P_{fa}=\int_{x_T}^{\infty}\int_{-\infty}^{\infty}\frac{1}{\sqrt{2\pi}\sigma}\exp\left[-\frac{(x-y)^2}{2\sigma^2}\right]P_{PD}(y|\mu_0)dydx \tag{10}$$

The double integrals in (10) can be simplified by first interchanging the orders of the integrals and then using the built-in error function of the computer. That is,

$$p_{fa}=\int_{-\infty}^{\infty}\left\{\int_{x_T}^{\infty}\frac{1}{\sqrt{2\pi}\sigma}\exp\left[-\frac{(x-y)^2}{2\sigma^2}\right]dx\right\}P_{PD}(y|\mu_0)dy=\int_{\mu_0}^{\infty}P_{PD}(y|\mu_0)\,\Phi\left(\frac{y-X_T}{\sigma}\right)dy \qquad (11)$$

where

$$\Phi(u)=\int_{-\infty}^{u}\frac{1}{\sqrt{2\pi}}\exp\left[-\frac{x^2}{2}\right]dx. \qquad (12)$$

Using the built-in complimentary error function,

$$\operatorname{erfc}(x)=1-\operatorname{erf}(x)=1-\int_0^x\frac{2}{\sqrt{\pi}}e^{-u^2}du$$

$$=1-\int_0^{\sqrt{2}x}\frac{2}{\sqrt{2\pi}}e^{-\frac{v^2}{2}}dv=\int_{\sqrt{2}x}^{\infty}\frac{2}{\sqrt{2\pi}}e^{-\frac{v^2}{2}}dv=2\Phi(-\sqrt{2}x)$$

or

$$\Phi(u)=\frac{1}{2}\operatorname{erfc}\left(-\frac{u}{\sqrt{2}}\right) \qquad (13)$$

Substituting (13) into (11)

$$p_{fa}=\int_{\mu_0}^{\infty}P_{PD}(y|\mu_0)\,\frac{1}{2}\operatorname{erfc}\left(\frac{X_T-y}{\sqrt{2}\sigma}\right)dy \qquad (14)$$

2. The program

Figure 1 shows a block diagram of the Fortran program which first evaluate Eq. (14) and then generate a Poisson random number with the mean given by Eq. (1). The subroutines and functions used for the numerical integration and Poisson random number generation are copied from those given in [6, ch. 4 and ch. 7].

References

[1] M. I. Skolnik, *Introduction to Radar Systems,* McGraw-Hill, New York, 1962, p. 31.

[2] R. J. McIntyre, "The distribution of gains in uniformly multiplying avalanche photodiodes: Theory," *IEEE Trans. Electron Devices*, Vol. ED-19, pp. 703-713, June 1972.

[3] J. Conradi, "The distribution of gains in uniformly multiplying avalanche photodiodes: Experimental," *IEEE Trans. Electron Devices*, Vol. ED-19, pp. 713-718, June 1972.

[4] P. P. Webb, R. J. McIntyre, and J. Conradi, "Property of avalanche photodiodes," *RCA Review*, Vol. 35, pp. 234-278, June 1974.

[5] F. M. Davidson and X. Sun, "Gaussian approximation versus nearly exact performance analysis of optical communication systems with PPM signaling and APD receivers," *IEEE Trans. Commun.* , Vol. COM-36, No. 11, pp. 1185-1192, Nov. 1988.

[6] W. H. Press, S. A. Teukolsky, W. T. Vetterling, and B. P. Flannery, *Numerical Recipes in Fortran: The Art of Scientific Computing*, 2nd Ed., Cambridge University Press, Cambridge, 1992.

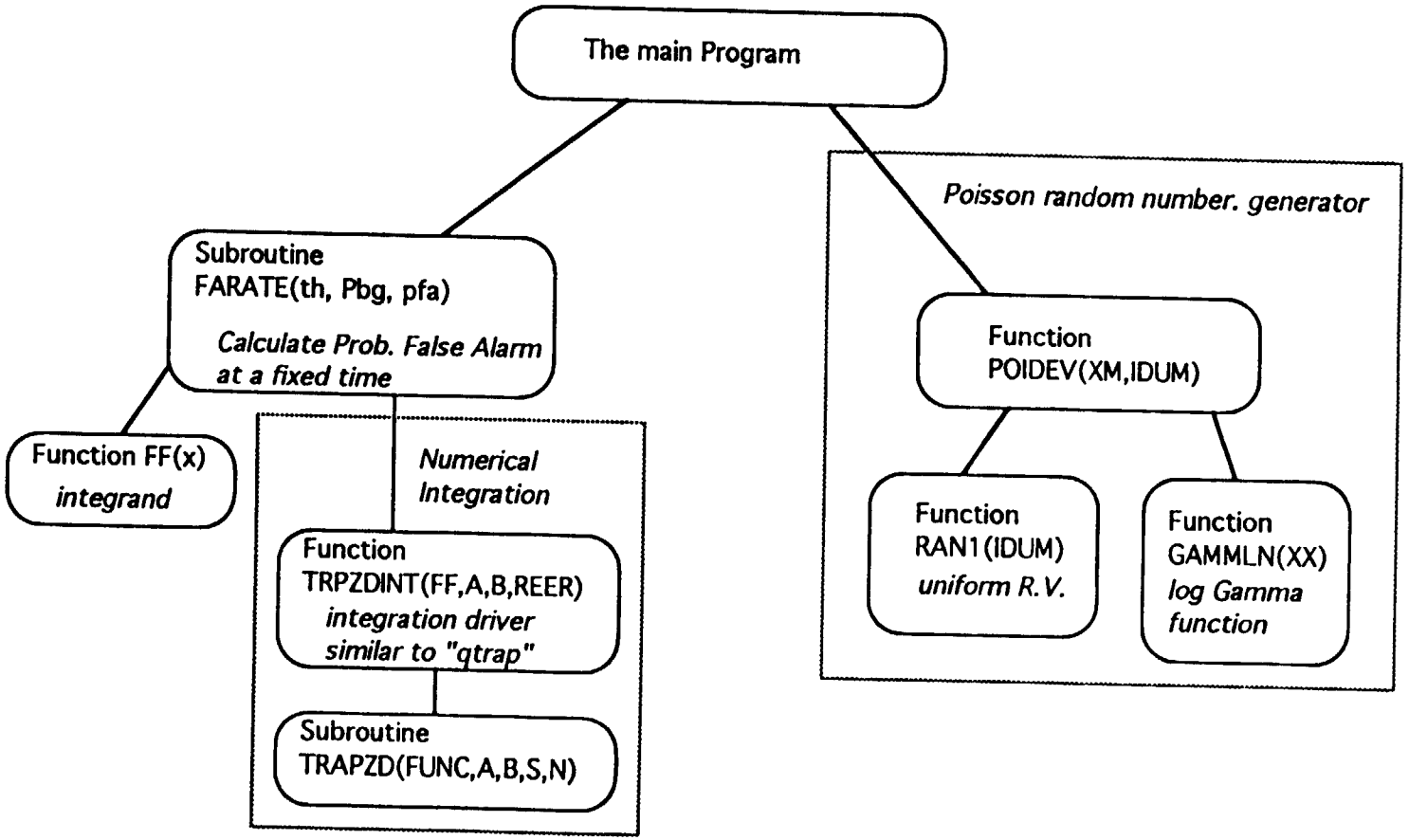

Figure 1. Block diagram of the program.

GLAS Altimeter Link Margin Analysis

Xiaoli Sun, The Johns Hopkins University

April 1994

Calculation of the detected signal and noise photons per pulse

$E_t := 0.040$ Laser transmitter pulse energy (J)

$i := 1..20$ Number of points to be calculated

$R_0 := 200$ $\Delta R := 50$ Initial range and step size

$R_i := \Delta R \cdot i + R_0$ Range to the target (km)

$r_{diff} := 0.2$ Target diffusion coefficient

$\phi_{tel} := 0.50$ Receiver Telescope Diameter (m)

$\theta_{FOV} := 0.850 \cdot 10^{-3}$ Receiver FOV (rad)

$\eta_{rcvr} := 0.5$ Receiver optics transmission

$\eta_{atmo} := 0.5$ Atmosphere Transmission Coefficient

$\eta_{APD} := 0.35$ APD quantum efficiency

$I_{solar} := 310$ Solar irradiance at the target (W/m^2/um)

$\Delta\lambda := 0.003$ Receiver optical bandwidth (um)

Solar background noise photons per second

$$P_b := I_{solar} \cdot \Delta\lambda \cdot \eta_{rcvr} \cdot \pi \cdot \left(\frac{\theta_{FOV}}{2}\right)^2 \cdot \frac{r_{diff}}{\pi} \cdot \left(\pi \cdot \frac{\phi_{tel}^2}{4}\right)$$

$$\lambda_b := \frac{\eta_{APD} \cdot P_b}{1.17 \cdot 1.6 \cdot 10^{-19}}$$

$P_b = 3.2983 \cdot 10^{-9}$ $\lambda_b = 6.1667 \cdot 10^{9}$

Signal photons per pulse

$$N_s(R) := \frac{E_t}{1.17 \cdot 1.6 \cdot 10^{-19}} \cdot \frac{r_{diff}}{\pi} \cdot \left[\pi \cdot \frac{\phi_{tel}^2}{4 \cdot (R \cdot 1000)^2}\right] \cdot \eta_{rcvr} \cdot \eta_{atmo} \cdot \eta_{APD}$$

R_i	$N_s(R_i)$
$2.5 \cdot 10^2$	$3.7393 \cdot 10^3$
$3 \cdot 10^2$	$2.5967 \cdot 10^3$
$3.5 \cdot 10^2$	$1.9078 \cdot 10^3$
$4 \cdot 10^2$	$1.4607 \cdot 10^3$
$4.5 \cdot 10^2$	$1.1541 \cdot 10^3$
$5 \cdot 10^2$	$9.3483 \cdot 10^2$
$5.5 \cdot 10^2$	$7.7259 \cdot 10^2$
$6 \cdot 10^2$	$6.4919 \cdot 10^2$
$6.5 \cdot 10^2$	$5.5315 \cdot 10^2$
$7 \cdot 10^2$	$4.7695 \cdot 10^2$
$7.5 \cdot 10^2$	$4.1548 \cdot 10^2$
$8 \cdot 10^2$	$3.6517 \cdot 10^2$
$8.5 \cdot 10^2$	$3.2347 \cdot 10^2$
$9 \cdot 10^2$	$2.8853 \cdot 10^2$
$9.5 \cdot 10^2$	$2.5896 \cdot 10^2$
$1 \cdot 10^3$	$2.3371 \cdot 10^2$
$1.05 \cdot 10^3$	$2.1198 \cdot 10^2$
$1.1 \cdot 10^3$	$1.9315 \cdot 10^2$
$1.15 \cdot 10^3$	$1.7672 \cdot 10^2$
$1.2 \cdot 10^3$	$1.623 \cdot 10^2$

Other system parameter values:

$\tau := 20 \cdot 10^{-9}$ Laser pulse width

$R_G := 20$ Range gate (km)

$T := 2 \cdot \frac{R_G \cdot 1000}{3 \cdot 10^8}$ Range gate interval (sec) $T = 1.3333 \cdot 10^{-4}$

$n_b := \lambda_b \cdot \tau$ Detected background noise photons per pulse interval

$I_s := 15 \cdot 10^{-9}$ APD surface leakage current (A)

$I_b := 50 \cdot 10^{-12}$ APD bulk leakage current (A)

$G := 200$ Average APD gain

$k_{eff} := 0.01$ APD ionization coefficient ratio

$R_l := 20000$ Preamp feedback resistance (ohm)

$T_n := 700$ Preamp equivalent noise temperature (Kelvin)

The means of the APD outputs:

$$\mu_0 := \left(n_b + \frac{I_b}{1.6 \cdot 10^{-19}} \cdot \tau \right)$$

$\mu_0 = 1.2958 \cdot 10^2$ $n_b = 1.2333 \cdot 10^2$ $\frac{I_b}{1.6 \cdot 10^{-19}} \cdot \tau = 6.25$

$\mu_1(n_s) := n_s + \mu_0$

The variance of the preamplifier noise and APD surface leakage current noise:

$$var := \left[\frac{2 \cdot 1.38 \cdot 10^{-23} \cdot T_n \cdot \tau}{R_l \cdot (1.6 \cdot 10^{-19})^2} + \frac{I_s \cdot \tau}{1.6 \cdot 10^{-19}} \right]$$

$\sigma := \sqrt{var}$

$\sigma = 8.6981 \cdot 10^2$ $\frac{\sigma}{G} = 4.349$ $\frac{\sqrt{\frac{2 \cdot 1.38 \cdot 10^{-23} \cdot T_n \cdot \tau}{R_l \cdot (1.6 \cdot 10^{-19})^2}}}{G} = 4.3436$ $\frac{\sqrt{\frac{I_s \cdot \tau}{1.6 \cdot 10^{-19} \cdot G}}}{G} = 0.0153$

The p.d.f. of the APD output:

$$F := k_{eff} \cdot G + \left(2 - \frac{1}{G}\right) \cdot (1 - k_{eff})$$

$F = 3.9751$ APD excess noise factor

$$s_{00} := \sqrt{G^2 \cdot F \cdot \mu_0} \qquad s_{00} = 4.5392 \cdot 10^3$$

$$P_{PD0}(z) := \frac{1}{\sqrt{2 \cdot \pi}} \cdot \frac{1}{\left[1 + \frac{G \cdot (F-1) \cdot z}{s_{00}}\right]^{\frac{3}{2}}} \cdot \exp\left[\frac{-z^2}{2 \cdot \left[1 + \frac{G \cdot (F-1) \cdot z}{s_{00}}\right]}\right]$$

$$s_{11}(n_s) := \sqrt{G^2 \cdot F \cdot \mu_1(n_s)}$$

$$P_{PD1}(z, n_s) := \frac{1}{\sqrt{2 \cdot \pi}} \cdot \frac{1}{\left[1 + \frac{G \cdot (F-1) \cdot z}{s_{11}(n_s)}\right]^{\frac{3}{2}}} \cdot \exp\left[\frac{-z^2}{2 \cdot \left[1 + \frac{G \cdot (F-1) \cdot z}{s_{11}(n_s)}\right]}\right]$$

Probabilities of false alarm:

$$s_0 := \sqrt{{s_{00}}^2 + \sigma^2} \qquad s_0 = 4.6218 \cdot 10^3$$

Standard deviation of the noise

$$z_0 := \frac{\mu_0 - G \cdot \mu_0}{s_{00}}$$

$z_0 = -5.681$ lower limit of the integral

$z_1 := 100$ Upper limit of the integral

$$p_{fa}(n_T) := \int_{z_0}^{z_1} P_{PD0}(z) \cdot \text{cnorm}\left(\frac{s_{00} \cdot z - n_T \cdot s_0}{\sigma}\right) dz$$

The built-in function "cnorm(u)" is the culmulative probability distribution function of a Gaussian r.v. with zero mean and unity variance

$$P_{FA}(n_T) := 1 - \exp\left(-\frac{T}{\tau} \cdot p_{fa}(n_T)\right)$$

The probability of correct detection:

$$z_{01}(n_s) := \frac{\mu_1(n_s) - G \cdot \mu_1(n_s)}{s_{11}(n_s)}$$

$$z_{01}(10) = -5.8962$$

$$z_{11} := 100$$

$$P_D(n_s, n_T) := \int_{z_{01}(n_s)}^{z_{11}} P_{PD1}(z, n_s) \cdot \text{cnorm}\left[\frac{s_{11}(n_s) \cdot z - n_T \cdot s_0 + G \cdot (\mu_1(n_s) - \mu_0)}{\sigma}\right] dz$$

$k := 0, 1 .. 10$

$NT_k := 5 + 0.5 \cdot k$ Normalized threshold level

$TOL := 10^{-12}$ The integration error tolerance

$pfa_k := p_{fa}(NT_k)$

$PFA_k := 1 - \exp\left(-\frac{T}{\tau} \cdot pfa_k\right)$

NT_k	pfa_k	PFA_k
5	$3.3545 \cdot 10^{-5}$	0.2004
5.5	$8.6669 \cdot 10^{-6}$	0.0561
6	$2.1431 \cdot 10^{-6}$	0.0142
6.5	$5.0946 \cdot 10^{-7}$	$3.3906 \cdot 10^{-3}$
7	$1.1689 \cdot 10^{-7}$	$7.7894 \cdot 10^{-4}$
7.5	$2.5971 \cdot 10^{-8}$	$1.7313 \cdot 10^{-4}$
8	$5.6053 \cdot 10^{-9}$	$3.7368 \cdot 10^{-5}$
8.5	$1.1783 \cdot 10^{-9}$	$7.8552 \cdot 10^{-6}$
9	$2.4181 \cdot 10^{-10}$	$1.612 \cdot 10^{-6}$
9.5	$4.8545 \cdot 10^{-11}$	$3.2364 \cdot 10^{-7}$
10	$9.5513 \cdot 10^{-12}$	$6.3675 \cdot 10^{-8}$

$TOL := 10^{-7}$

R_i	$N_s(R_i)$	$P_D(N_s(R_i), 7.0)$
$2.5 \cdot 10^2$	$3.7393 \cdot 10^3$	1
$3 \cdot 10^2$	$2.5967 \cdot 10^3$	1
$3.5 \cdot 10^2$	$1.9078 \cdot 10^3$	1
$4 \cdot 10^2$	$1.4607 \cdot 10^3$	1
$4.5 \cdot 10^2$	$1.1541 \cdot 10^3$	1
$5 \cdot 10^2$	$9.3483 \cdot 10^2$	1
$5.5 \cdot 10^2$	$7.7259 \cdot 10^2$	1
$6 \cdot 10^2$	$6.4919 \cdot 10^2$	1
$6.5 \cdot 10^2$	$5.5315 \cdot 10^2$	1
$7 \cdot 10^2$	$4.7695 \cdot 10^2$	1
$7.5 \cdot 10^2$	$4.1548 \cdot 10^2$	0.9997
$8 \cdot 10^2$	$3.6517 \cdot 10^2$	0.9964
$8.5 \cdot 10^2$	$3.2347 \cdot 10^2$	0.9771
$9 \cdot 10^2$	$2.8853 \cdot 10^2$	0.9183
$9.5 \cdot 10^2$	$2.5896 \cdot 10^2$	0.8058
$1 \cdot 10^3$	$2.3371 \cdot 10^2$	0.6524
$1.05 \cdot 10^3$	$2.1198 \cdot 10^2$	0.4893
$1.1 \cdot 10^3$	$1.9315 \cdot 10^2$	
$1.15 \cdot 10^3$	$1.7672 \cdot 10^2$	
$1.2 \cdot 10^3$	$1.623 \cdot 10^2$	

GLAS Cloud Lidar Receiver Photon Count Rate Calculation

Xiaoli Sun, Johns Hopkins University, March 1994

Instrument parameters:

Laser pulse energy (Joule/pulse):	$E_t := 0.050$
Laser wavelength (nm):	$\lambda := 532$
Laser pulsewidth (s):	$\tau := 20 \cdot 10^{-9}$
Laser pulse repetition rate (Hz):	$F_p := 40$
Laser beam divergence angle (rad):	$\theta_d := 100 \cdot 10^{-6}$
Lidar altitude (m):	$R := 705 \cdot 10^{3}$
Receiver optics FOV (rad):	$\theta_{FOV} := 250 \cdot 10^{-6}$
Receiver telescope diameter (m):	$\phi_{tel} := 0.90$
Telescope secondary mirror diameter (m):	$\phi_{obs} := 0.20$
Total transmission of the receiver optics:	$T_0 := 0.5$
Receiver optical bandwidth (nm):	$\Delta\lambda := 0.10$
Range gate (km):	$RG := 20$
PMT quantum efficiency:	$\eta := 0.20$
PMT gain:	$G := 10^{5}$
PMT dark counts/s:	$nd_{PMT} := 150$
Receiver photon counting interval (s):	$\Delta t := 0.5 \cdot 10^{-6}$
electron charge (C):	$q := 1.6 \cdot 10^{-19}$
Speed of light (m/s):	$c := 3 \cdot 10^{8}$
Photon energy (Joule):	$hf := \frac{1242}{\lambda} \cdot 1.6 \cdot 10^{-19}$
Range gate interval (s):	$T_{RG} := \frac{RG \cdot 10^{3}}{c} \cdot 2$ $\quad T_{RG} = 1.333 \cdot 10^{-4}$

Atmosphere parameter values at 532 nm wavelength:

Solar spectral irradiance (W/m^2 um): $E_{\lambda solar} := 1848$

Lunar Spectral irradiance (W/m^2 um): $E_{\lambda lunar} := 0.0044$

Albedo of the terrain: $r_{ter} := 0.34$

Albedo of the cloud: $r_{cloud} := 0.70$

Spectral radiance intensity of terrian at daytime (uW/cm^2 um sr):

$$I_{day} := \left(E_{\lambda solar} \cdot 10^2\right) \cdot \frac{r_{ter}}{\pi} \qquad I_{day} = 2 \cdot 10^4$$

Spectral radiance intensity of sunlit cloud (uW/cm^2 um sr):

$$I_{daycloud} := \left(E_{\lambda solar} \cdot 10^2\right) \cdot \frac{r_{cloud}}{\pi} \qquad I_{daycloud} = 4.118 \cdot 10^4$$

Maximum spectral radiance intensity at night at full moon (uW/cm^2 um sr):

$$I_{night} := \left(E_{\lambda lunar} \cdot 10^2\right) \cdot \frac{r_{cloud}}{\pi} \qquad I_{night} = 0.098$$

Aerosol cross section times the square of the atmosphere transmission (1/km sr) as a function of altitude (km):

$i := 0, 1 .. 48$ $\quad HT := READPRN(GLASHT)$ $\quad \beta T2 := READPRN(GLASBTT)$

$\beta TT(h) := linterp(HT, \beta T2, h)$ $\quad h := 0.1, 0.2 .. 25$

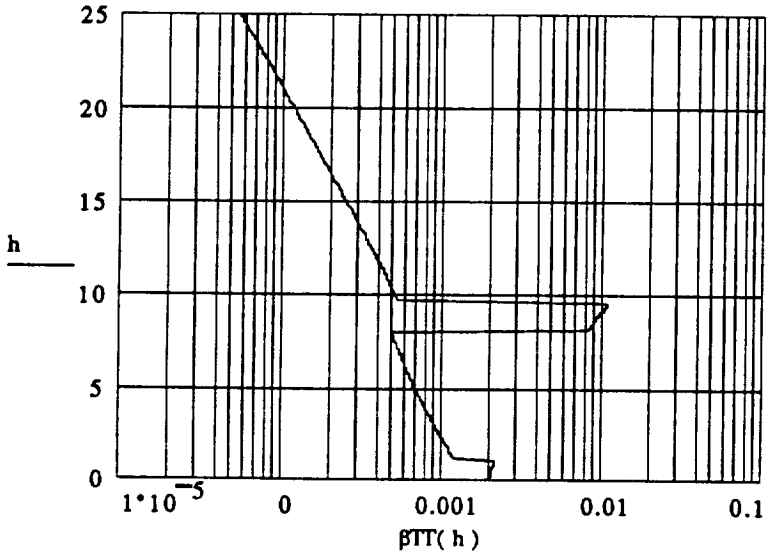

Calculated Results

Received signal photons/s:

Received laser signal power (Watts):

$$P_r(h) := \frac{c}{2} \cdot E_t \cdot \frac{\pi \cdot \left(\phi_{tel}^2 - \phi_{obs}^2\right)}{4 \cdot (R - h \cdot 1000)^2} \cdot T_0 \cdot (\beta TT(h) \cdot 10^{-3})$$

Peak signal (Watts) (at 9.5 km altitude): $P_r(9.5) = 5.1572 \cdot 10^{-11}$

Detecteded signal photons/s as a function of the cloud altitude in km:

$$n_s(h) := \eta \cdot \frac{P_r(h)}{hf} \qquad n_s(9.5) = 2.761 \cdot 10^7$$

Detected signal photons/s as a function of time:

Reflection from the ground:

$$n1_s(t) := \text{if}\left[t \geq \left(2 \cdot \frac{R}{c} + \tau\right), 0, \frac{E_t}{\tau} \cdot \frac{r_{ter}}{\pi} \cdot \frac{\pi \cdot \left(\phi_{tel}^2 - \phi_{obs}^2\right)}{4 \cdot R^2} \cdot 0.5 \cdot T_0 \cdot \Phi\left(t - 2 \cdot \frac{R}{c}\right) \cdot \frac{\eta}{hf}\right]$$

Total signal photons/s: $n1_s\left(2 \cdot \frac{R}{c} + 10^{-8}\right) = 4.407 \cdot 10^{10}$

$$ns(t) := \text{if}\left[t > \left(2 \cdot \frac{R}{c} + 20 \cdot 10^{-9}\right), 0, n_s\left[\left(R - \frac{c \cdot t}{2}\right) \cdot 10^{-3}\right] + n1_s(t)\right]$$

Background radiation noise photons/s:

Receiver FOV solid angle:

$$\Omega := \frac{\pi \cdot \theta_{FOV}^2}{4}$$

Day time:

Clear Sky:

$$PB_d := \left(I_{day} \cdot 10^{-6}\right) \cdot \frac{\pi \cdot \left(\phi_{tel}^2 - \phi_{obs}^2\right) \cdot 10^4}{4} \cdot T_0 \cdot \Omega \cdot (\Delta\lambda \cdot 10^{-3}) \qquad PB_d = 2.969 \cdot 10^{-10}$$

$$nb_d := \eta \cdot \frac{PB_d}{hf} \qquad nb_d = 1.589 \cdot 10^8$$

Bright cloud:

$$PB_{dcloud} := \left(I_{daycloud} \cdot 10^{-6}\right) \cdot \frac{\pi \cdot \left(\phi_{tel}^2 - \phi_{obs}^2\right) \cdot 10^4}{4} \cdot T_0 \cdot \Omega \cdot (\Delta\lambda \cdot 10^{-3})$$

$$nb_{dcloud} := \eta \cdot \frac{PB_{dcloud}}{hf} \qquad PB_{dcloud} = 6.112 \cdot 10^{-10}$$

$$nb_{dcloud} = 3.272 \cdot 10^8$$

Night time with cloud at full moon:

$$PB_n := \left(I_{night} \cdot 10^{-6}\right) \cdot \frac{\pi \cdot \left(\phi_{tel}^2 - \phi_{obs}^2\right) \cdot 10^4}{4} \cdot T_0 \cdot \Omega \cdot (\Delta\lambda \cdot 10^{-3})$$

$$nb_n := \eta \cdot \frac{PB_n}{hf}$$

$$PB_n = 1.455 \cdot 10^{-15}$$

$$nb_n = 779.151$$

Maximum PMT current (A):

Cathod: $I_{PMTc} := (nb_{dcloud} + n_s(9.5)) \cdot q$ $I_{PMTc} = 5.678 \cdot 10^{-11}$

Anode: $I_{PMTa} := I_{PMTc} \cdot G$ $I_{PMTa} = 5.678 \cdot 10^{-6}$

Upper bonds for the total electron charge drawn from the PMT photocathod:

Average number of detected photons per 24 hours with the range gate:

$$N := \left[n_s(9.5) + 0.5 \cdot \left(\frac{nb_d}{\frac{\pi}{2}} \right) + 0.5 \cdot nb_n \right] \cdot T_{RG} \cdot F_p \cdot 3600 \cdot 24 \qquad N = 3.604 \cdot 10^{10}$$

If there were always bright clouds:

$$N_c := \left[n_s(9.5) + 0.5 \cdot \left(\frac{nb_{dcloud}}{\frac{\pi}{2}} \right) + 0.5 \cdot nb_n \right] \cdot T_{RG} \cdot F_p \cdot 3600 \cdot 24 \qquad N_c = 6.072 \cdot 10^{10}$$

Average number of detected photons per day with NO range gate:

$$N_{NRG} := \left[n_s(9.5) + 0.5 \cdot \left(\frac{nb_d}{\frac{\pi}{2}} \right) + 0.5 \cdot nb_n \right] \cdot 3600 \cdot 24 \qquad N_{NRG} = 6.757 \cdot 10^{12}$$

If there were always bright clouds:

$$N_{NRGcloud} := \left[n_s(9.5) + 0.5 \cdot \left(\frac{nb_{dcloud}}{\frac{\pi}{2}} \right) + 0.5 \cdot nb_n \right] \cdot 3600 \cdot 24 \qquad N_{NRGcloud} = 1.139 \cdot 10^{13}$$

Total number detected photons over the GLAS 5 year mission:

With range gate:

$$N_{5yr} := N_c \cdot 5 \cdot 365 \qquad N_{5yr} = 1.108 \cdot 10^{14}$$

With NO range gate:

$$N_{NRG5yr} := N_{NRGcloud} \cdot 5 \cdot 365 \qquad N_{NRG5yr} = 2.078 \cdot 10^{16}$$

Total electron charges drawn from the PMT photocathod (Coulomb):

With range gate:

$$C_{cathod} := N_{5yr} \cdot 1.6 \cdot 10^{-19} \qquad C_{cathod} = 1.773 \cdot 10^{-5}$$

Without range gate:

$$C_{NRGcathod} := N_{NRG5yr} \cdot 1.6 \cdot 10^{-19} \qquad C_{NRGcathod} = 0.00332$$

Total Detected Photons per sec:

$J := 500 \qquad j := 0..300 \qquad t_j := \left[\left(j \cdot 10^{-6} - J \cdot 0.4 \cdot 10^{-6} \right) + \frac{R}{c} \cdot 2 \right]$

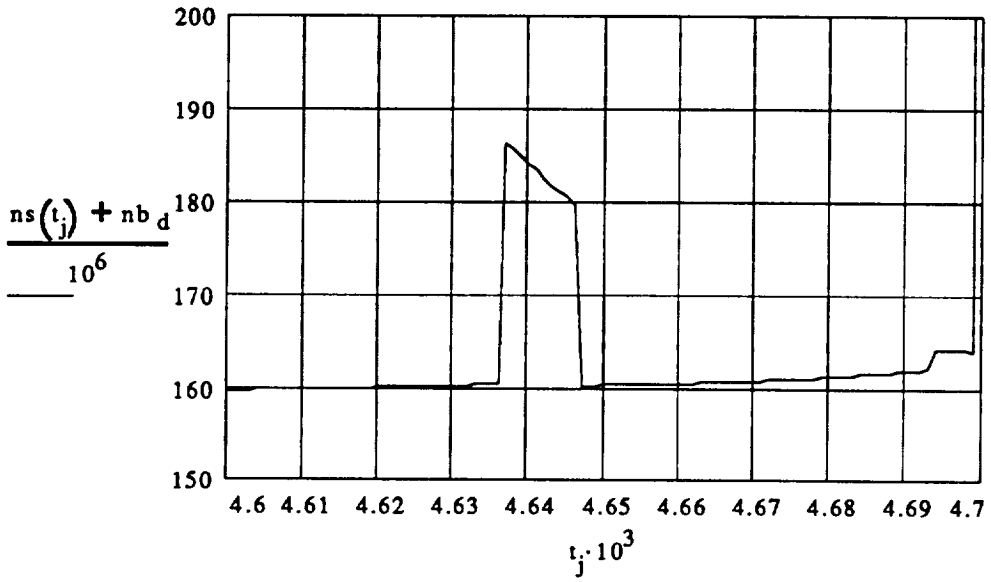

Time from the laser pulse (ms)

Receiver Signal to Noise Ratio Calculation:

Number of laser shot averaged: $NL := 1$

$$SNR_d(h) := \frac{NL \cdot n_s(h) \cdot \Delta t}{\sqrt{(n_s(h) + nb_d + nd_{PMT}) \cdot \Delta t \cdot NL}} \qquad SNR_n(h) := \frac{n_s(h) \cdot \Delta t \cdot NL}{\sqrt{(n_s(h) + nb_n + nd_{PMT}) \cdot \Delta t \cdot NL}}$$

Day and Night
SNR vs. h

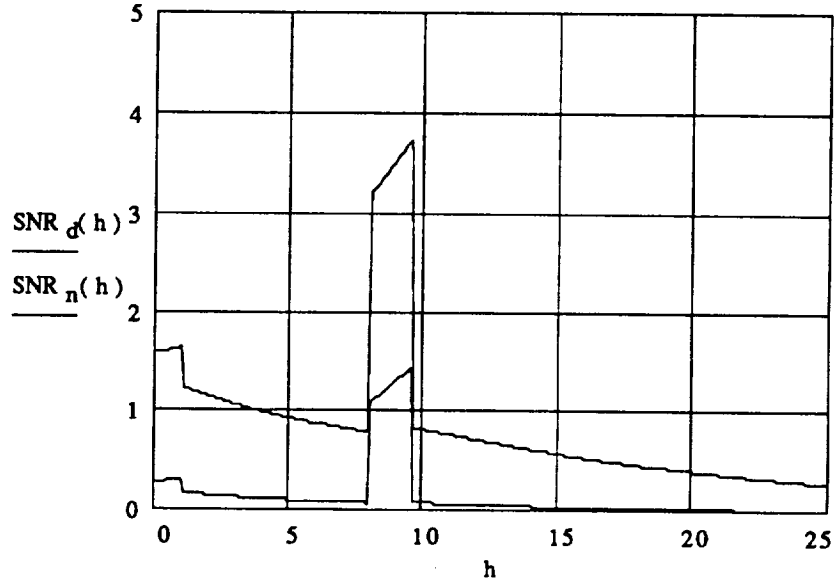

Cloud Altitude (km)

Use of the NRAO Method† for the GAMES Fine Ranging Receiver

Xiaoli Sun
The Johns Hopkins University
Baltimore, Maryland 21218-2686

February 1994

1. Analysis of Phase Estimation Bias due to Doppler Shift.

The average received analog signal from an ideal photodetector may be written as

$$x_o(t) = A\cos[(\omega_c + \omega_D)t + \theta] \tag{1}$$

The actual signal into the computer is the truncated and digitized signal given in (1) and it can be written as

$$x(t) = \sum_{n=n_0}^{N+n_0} x_n \delta(t - n\Delta t) = w(t) \cdot \left(\sum_{n=-\infty}^{\infty} \delta(t - n\Delta t) \right) \cdot x_o(t) \tag{2}$$

where

$$w(t) = \begin{cases} 1, & t_o \le t \le T + t_o \\ 0, & Otherwise \end{cases}, \qquad N = \frac{\Delta t}{T} \tag{3}$$

and

$$x_n = x_o(n\Delta t) = A\cos[(\omega_c + \omega_D)n\Delta t + \theta] \tag{4}$$

---

† J. M. Payne, D. Parker, and R. F. Bradley (National Radio Astronomy Observatory, Charlottesville, VA 22903), "Range finder with fast multiple range capability," *Rev. Sci. Instrum.*, Vol. 63, No. 6, pp. 3311-3316, June 1992.

The phase esitmator using the NRAO method is given by

$$\hat{\theta} = \tan^{-1}\left\{\frac{\mathrm{Im}[X(\omega_c)]}{\mathrm{Re}[X(\omega_c)]}\right\} = \tan^{-1}\left[\frac{\sum_{n=n_0}^{N+n_0} x_n \sin(\omega_c n\Delta t)}{\sum_{n=n_0}^{N+n_0} x_n \cos(\omega_c n\Delta t)}\right] \tag{5}$$

where

$$\begin{aligned} X(\omega_c) &= \int_{-\infty}^{\infty} x(t) e^{-j\omega_c t} dt \\ &= \sum_{n=n_0}^{N+n_0} x_n \int_{-\infty}^{\infty} e^{-j\omega_c t}\delta(t - n\Delta t)dt \\ &= \sum_{n=n_0}^{N+n_0} x_n \cos(\omega_c n\Delta t) + j\sum_{n=n_0}^{N+n_0} x_n \sin(\omega_c n\Delta t) \end{aligned} \tag{6}$$

Eq. (6) should also be equal to the Fourier transform of the right hand side of Eq. (2) which can be written as the convolution of the Fourier transforms of the rectangular window function, the sample function, and the signal, as

$$X(\omega) = W(\omega) * \left(\frac{2\pi}{\Delta t}\sum_{k=-\infty}^{\infty}\delta(\omega - k\frac{2\pi}{\Delta t})\right) * X_o(\omega) \tag{7}$$

Since

$$W(\omega) = T \cdot sinc\left(\frac{\omega T}{2}\right)\cdot e^{-j\omega x_o} \tag{8}$$

and

$$X_o(\omega) = \frac{A}{2}\left\{e^{j\theta}\delta[\omega - (\omega_c + \omega_D)] + e^{-j\theta}\delta[\omega + (\omega_c + \omega_D)]\right\}, \tag{9}$$

therefore

$$X(\omega)=\frac{\pi TA}{\Delta t}\left\{\sum_{k=-\infty}^{\infty} sinc[\frac{(\omega-k\frac{2\pi}{\Delta t})T}{2}]\, e^{-j(\omega-k\frac{2\pi}{\Delta t})t_0}\right\}$$

$$*\left\{e^{j\theta}\delta[\omega-(\omega_c+\omega_D)]+e^{-j\theta}\delta[\omega+(\omega_c+\omega_D)]\right\} \qquad (10)$$

$$X(\omega)=\frac{\pi TA}{\Delta t}\left\{e^{j\theta}\sum_{k=-\infty}^{\infty} sinc\left[\frac{(\omega-(\omega_c+\omega_D)-k\frac{2\pi}{\Delta t})T}{2}\right] e^{-j(\omega-(\omega_c+\omega_D)-k\frac{2\pi}{\Delta t})t_0}\right.$$

$$\left.+e^{-j\theta}\sum_{k=-\infty}^{\infty} sinc\left[\frac{(\omega+(\omega_c+\omega_D)-k\frac{2\pi}{\Delta t})T}{2}\right] e^{-j(\omega+(\omega_c+\omega_D)-k\frac{2\pi}{\Delta t})t_0}\right\} \qquad (11)$$

Assuming $\frac{2\pi}{\Delta t} >> \omega_c+\omega_D$ and filtering out all the $k\neq 0$ terms,

$$X(\omega)=\frac{\pi TA}{\Delta t}\left\{e^{j\theta}\, sinc(\frac{\omega_D T}{2})\, e^{j\omega_D t_0}\right.$$

$$\left.+e^{-j\theta}\, sinc\left[\frac{(2\omega_c+\omega_D)T}{2}\right] e^{-j(2\omega_c+\omega_D)t_0}\right\} \qquad (12)$$

The phase esitmator becomes

$$\hat{\theta}=tan^{-1}\left\{\frac{Im[X(\omega_c)]}{Re[X(\omega_c)]}\right\}$$

$$=tan^{-1}\left\{\frac{sin(\omega_D t_0+\theta)sinc(\frac{\omega_D T}{2})-sin[(2\omega_c+\omega_D)t_0+\theta]\, sinc\left[\frac{(2\omega_c+\omega_D)T}{2}\right]}{cos(\omega_D t_0+\theta)sinc(\frac{\omega_D T}{2})+cos[(2\omega_c+\omega_D)t_0+\theta]\, sinc\left[\frac{(2\omega_c+\omega_D)T}{2}\right]}\right\} \qquad (13)$$

If one select t_o such that $2\omega_c t_0=2m\pi$ with any integer m, then

$$\sin[\theta + (2\omega_c + \omega_D)t_0] = \sin(\theta + \omega_D t_0) \tag{14}$$

and

$$\hat{\theta} = \tan^{-1}\left\{\frac{\sin(\omega_D t_0 + \theta)\,sinc(\frac{\omega_D T}{2}) - \sin(\omega_D t_0 + \theta)\,sinc\left[\frac{(2\omega_c + \omega_D)T}{2}\right]}{\cos(\omega_D t_0 + \theta)\,sinc(\frac{\omega_D T}{2}) + \cos(\omega_D t_0 + \theta)\,sinc\left[\frac{(2\omega_c + \omega_D)T}{2}\right]}\right\}$$

$$= \tan^{-1}\left\{\tan(\omega_D t_0 + \theta)\cdot\frac{\frac{\sin(\omega_D T/2)}{\omega_D T/2} - \frac{\sin[(2\omega_c + \omega_D)T/2]}{(2\omega_c + \omega_D)T/2}}{\frac{\sin(\omega_D T/2)}{\omega_D T/2} + \frac{\sin[(2\omega_c + \omega_D)T/2]}{(2\omega_c + \omega_D)T/2}}\right\} \tag{15}$$

If $\omega_c T = 2n\pi$ for any integer n, $\sin[\frac{(2\omega_c + \omega_D)T}{2}] = \sin(\frac{\omega_D T}{2})$ and

$$\hat{\theta} = \tan^{-1}\left\{\tan(\omega_D t_0 + \theta)\cdot\frac{\frac{1}{\omega_D} - \frac{1}{(2\omega_c + \omega_D)}}{\frac{1}{\omega_D} + \frac{1}{(2\omega_c + \omega_D)}}\right\}$$

$$= \tan^{-1}\left\{\tan(\omega_D t_0 + \theta)\cdot\frac{\omega_c}{\omega_c + \omega_D}\right\} \tag{16}$$

or

$$\tan\hat{\theta} = \tan(\omega_D t_0 + \theta)\cdot\frac{\omega_c}{\omega_c + \omega_D} \tag{17}$$

The relative error in $\tan\hat{\theta}$ is given by

$$\varepsilon_{tan} = \frac{\tan\hat{\theta} - \tan(\omega_D t_0 + \theta)}{\tan(\omega_D t_0 + \theta)} = \frac{\omega_D}{\omega_c + \omega_D} \approx \frac{\omega_D}{\omega_c}, \qquad (\omega_D << \omega_c) \tag{18}$$

Since $d\tan\hat{\theta} = \frac{d\hat{\theta}}{\cos\hat{\theta}}$, the phase estimation error can be written as

$$\Delta\hat{\theta} \approx \cos\hat{\theta}\cdot\Delta\tan\hat{\theta} = \cos\hat{\theta}\cdot\tan(\omega_D t_0+\theta)\cdot\frac{\tan\hat{\theta}-\tan(\omega_D t_0+\theta)}{\tan(\omega_D t_0+\theta)}$$

$$\approx \cos(\omega_D t_0+\theta)\cdot\tan(\omega_D t_0+\theta)\cdot\frac{\omega_D}{\omega_c+\omega_D} \qquad (19)$$

$$\approx \frac{\omega_D}{\omega_c}\sin(\omega_D t_0+\theta)$$

The relative phase error is given by

$$\varepsilon_{\hat{\theta}} = \left|\frac{\Delta\hat{\theta}}{\omega_D t_0+\theta}\right| \approx \left|\frac{\omega_D}{\omega_c}\cdot\frac{\sin(\omega_D t_0+\theta)}{\omega_D t_0+\theta}\right| \le \left|\frac{\omega_D}{\omega_c}\right|, \qquad (|\omega_D| << \omega_c) \qquad (20)$$

An unbiased phase estimator is suggested according to (16), as

$$\hat{\theta}_0 = \tan^{-1}\left[\frac{\omega_c+\hat{\omega}_D}{\omega_c}\cdot\frac{\sum_{n=n_0}^{N+n_0} x_n\sin(\omega_c n\Delta t)}{\sum_{n=n_0}^{N+n_0} x_n\cos(\omega_c n\Delta t)}\right]. \qquad (21)$$

where $\hat{\omega}_D$ is the estimated Doppler shift obtained from the previous measurement.

2. Minimum Required Sampling Rate

The sampling rate after the down converter has to be fast enough to avoid aliasing. The Fourier transform of the sampled signal is given by Eq. (11) and it is plotted in Figure 1. It is obvious that the sampling rate should be such that

$$\frac{2\pi}{\Delta t} - 2(\omega_c+\omega_D) >> \frac{2\pi}{T} \qquad (22)$$

For GAMES, the carrier frequency is 10 KHz ($\omega_c = 2\pi\times10^4$) and, the maximum Doppler shift is a few Hertz, and the observation time is T=0.1s,

a sample rate of 3 times the carrier frequency, or 30 Ks/s, will be sufficient.

3. Quantization Caused by the A-to-D Converter

Quantization errors result from the limited resolution of the A-to-D converter. In this section, we analyze the maximum quantization error assuming there is no Doppler shift.

Considering the quantization error, the phase estimator given in Eq. (5) should be rewritten as

$$\begin{aligned}\hat{\theta}' &= \tan^{-1}\left[\frac{\sum_{n=n_0}^{N+n_0}(x_n+\Delta x_n)\sin(\omega_c n\Delta t)}{\sum_{n=n_0}^{N+n_0}(x_n+\Delta x_n)\cos(\omega_c n\Delta t)}\right] \\ &= \tan^{-1}\left[\frac{\sum_{n=n_0}^{N+n_0}x_n\sin(\omega_c n\Delta t)+\sum_{n=n_0}^{N+n_0}\Delta x_n\sin(\omega_c n\Delta t)}{\sum_{n=n_0}^{N+n_0}x_n\cos(\omega_c n\Delta t)+\sum_{n=n_0}^{N+n_0}\Delta x_n\cos(\omega_c n\Delta t)}\right]\end{aligned} \tag{23}$$

where Δx_n's are the quantization errors. One needs only to consider the case when $\hat{\theta}' \approx 0$. Under this condition, $\sum_{n=n_0}^{N+n_0} x_n \sin(\omega_c n\Delta t) << \sum_{n=n_0}^{N+n_0} x_n \cos(\omega_c n\Delta t)$

$$\hat{\theta}' \approx \frac{\sum_{n=n_0}^{N+n_0}x_n\sin(\omega_c n\Delta t)}{\sum_{n=n_0}^{N+n_0}x_n\cos(\omega_c n\Delta t)} + \frac{\sum_{n=n_0}^{N+n_0}\Delta x_n\sin(\omega_c n\Delta t)}{\sum_{n=n_0}^{N+n_0}x_n\cos(\omega_c n\Delta t)} \tag{24}$$

If the resolution of the A-to-D converter is given as Δx, the maximum uncertainty of each sample is $0.5\Delta x$, or, $|\Delta x_n| \le \Delta x/2$, the phase error due to quantization error becomes

$$\Delta\hat{\theta} = \left|\hat{\theta}' - \hat{\theta}\right| \approx \left| \frac{\sum_{n=n_0}^{N+n_0} \Delta x_n \sin(\omega_c n\Delta t)}{\sum_{n=n_0}^{N+n_0} x_n \cos(\omega_c n\Delta t)} \right|$$

$$\leq \frac{\Delta x_n \sum_{n=n_0}^{N+n_0} \left|\sin(\omega_c n\Delta t)\right|}{\left|\sum_{n=n_0}^{N+n_0} x_n \cos(\omega_c n\Delta t)\right|} \approx \frac{\frac{\Delta x}{2}\int_{t_0}^{T+t_0} \left|\sin(\omega_c t)\right| dt}{A\left|\int_{t_0}^{T+t_0} \cos(\omega_c t + \theta)\cos(\omega_c t)\, dt\right|}$$

$$= \frac{\frac{\Delta x}{2} \cdot N \cdot 2 \cdot \frac{2}{\omega_c}}{A \cdot \frac{1}{2} \cdot \cos(\theta) \cdot T} = \frac{2\Delta x}{\pi A \cos(\theta)}$$

$$\approx \frac{2}{\pi} \cdot \frac{\Delta x}{A} \qquad (25)$$

where the observation interval, T, is set to $T=N\times(2\pi/\omega_C)$. For a given maximum allowed phase error, $\Delta\theta_{max}$ (rad), the resolution of the A-to-D converter has to satisfy

$$\Delta x \leq \frac{\pi}{2} A \cdot \Delta\theta_{max} \qquad (26)$$

The minimum number of bits required for the A-to-D converter is

$$N_{bits} = \log_2\left(\frac{A}{\Delta x}\right) \geq \log_2\left(\frac{\pi/2}{\Delta\theta_{max}}\right) \qquad (27)$$

For example, a 9 bits A-to-D converter will give a maximum phase quantization error of 3.1 mrad, or 1/2048 of a cycle, which is sufficient for GAMES (50 μm at 2 GHz which corresponds to 4.2 mrad or1/1500 cycle).

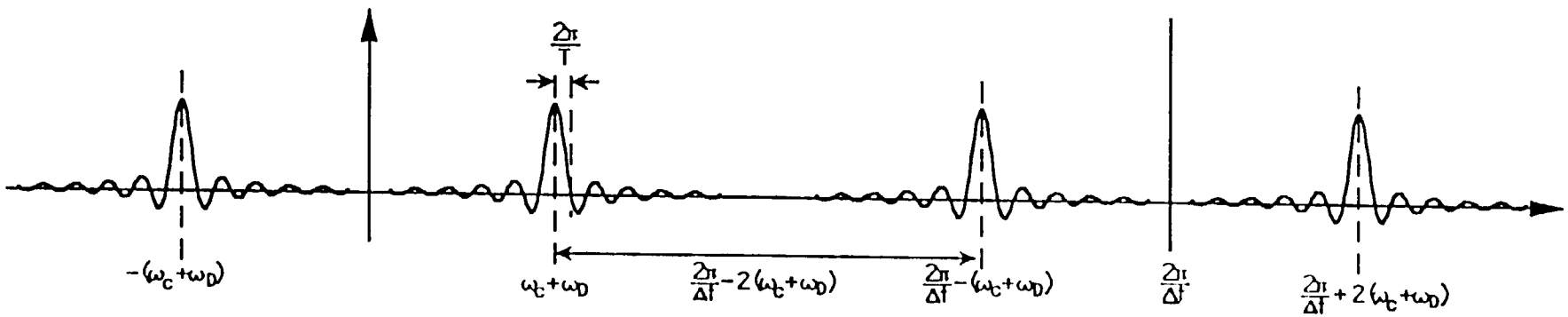

Figure 1. Fourier Transform of the Sampled Signal.

Receiver Performance Analysis of a Multiple Tone Laser Ranging System

System Block Diagram:

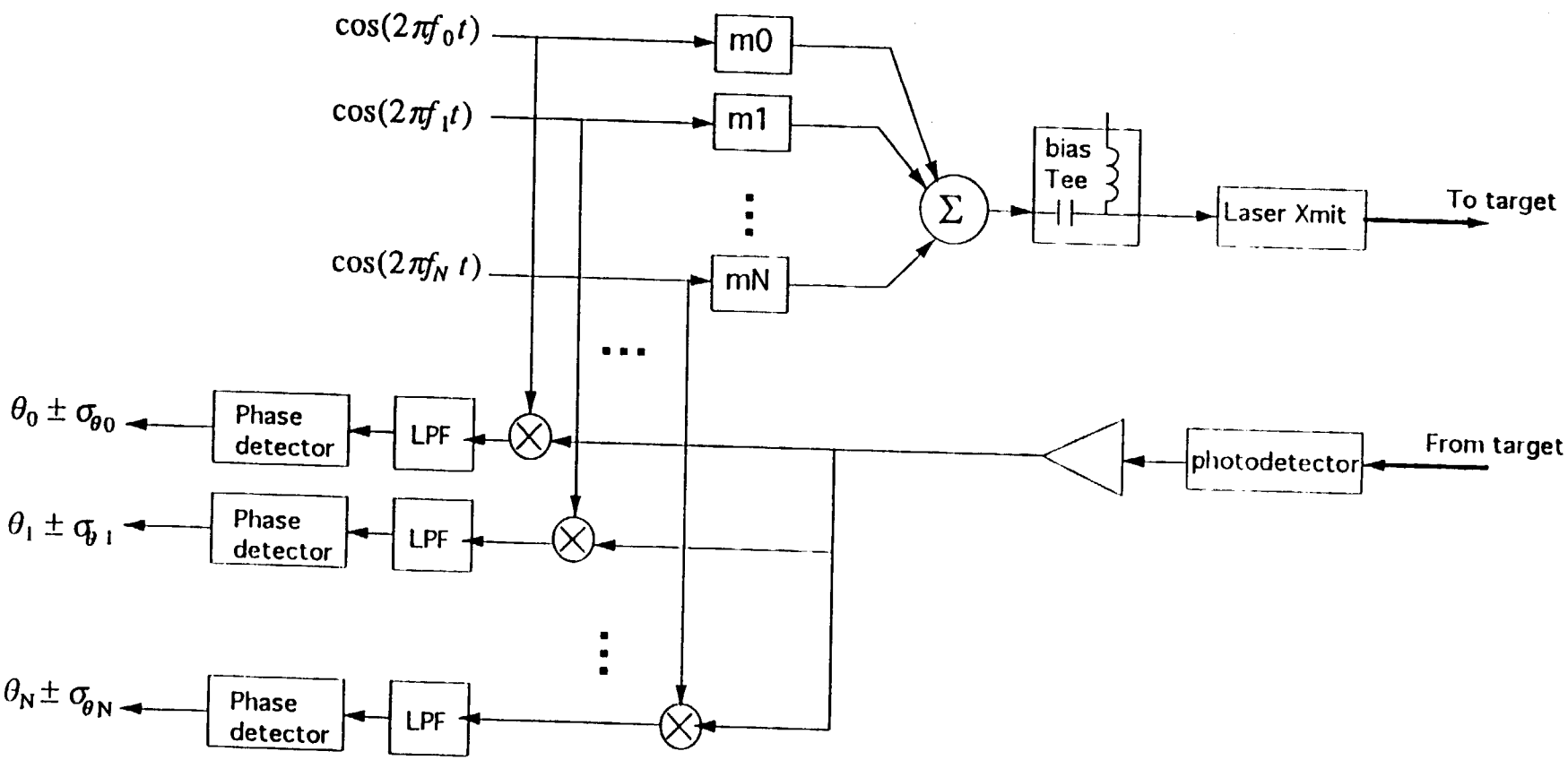

Principle of Operation:

- . $f_0 < f_1 < \cdots < f_N$
- Uncertainty in range for each tone: $\Delta R_i = \frac{1}{2}\frac{c}{f_i}$, $\Delta R_i < \Delta R_{i-1}$
- RMS Ranging error with f_i : $\sigma_i = \frac{\sigma_{\theta i}}{2\pi}\frac{c}{f_i}\frac{1}{2}$
- The phase error $\sigma_{\theta i}$ depends on SNRi but not the frequency of the tone
  If $SNR_i = SNR_{i-1}$ then $\sigma_{\theta i} = \sigma_{\theta(i-1)}$, and $\sigma_i < \sigma_{i-1}$

Choice of the Frequencies for the Tones:

- The range uncertainty of the i^{th} tone has to exceed the ranging error of the $i\text{-}1^{th}$ tone

i.e. $\Delta R_i > 2\sigma_{i-1}$ or $\frac{1}{2}\frac{c}{f_i} > 2\frac{\sigma_{\theta(i-1)}}{2\pi}\frac{c}{f_{i-1}}\frac{1}{2}$, $f_i < \frac{\pi}{\sigma_{\theta(i-1)}} f_{i-1}$

If $\frac{\sigma_{\theta i}}{\pi} < \frac{1}{2}$, one may choose $f_i = \frac{1}{2}\frac{\pi}{\sigma_{\theta(i-1)}} f_{i-1}$ (i.e. $\Delta R_i = 4\sigma_{i-1}$)

- . To satisfy the max range requirement: $f_0 < \frac{c}{2R_{max}}$
- To meets the system requirement, $\sigma_N = \frac{\sigma_{\theta N}}{2\pi}\frac{c}{f_N}\frac{1}{2} \le \sigma_R$

- Transmitted Signal:

$$P_{LD}(t) = (1-\alpha)\bar{P}_{LD} + \alpha\bar{P}_{LD}\left[m_0(1+\cos(2\pi f_0 t)) + m_1(1+\cos(2\pi f_1 t)) + \cdots + m_N(1+\cos(2\pi f_N t))\right]$$
$$= \bar{P}_{LD}\left[1+\alpha m_0\cos(2\pi f_0 t) + \alpha m_1\cos(2\pi f_1 t) + \cdots + \alpha m_N\cos(2\pi f_N t)\right]$$

where the modulation indices satisfy $m_0+m_1+ \ldots +m_N = 1$ and α is the fraction of laser power being modulated.

Average signal power: $E\{P_{LD}(t)\} = \bar{P}_{LD}$

Peak signal power: $\max\{P_{LD}(t)\} = \bar{P}_{LD}\left[1+\alpha m_0 + \alpha m_1 + \cdots + \alpha m_N\right] = (1+\alpha)\bar{P}_{LD} < 2\bar{P}_{LD}$

Receiver Performance:

- Range error of the ith tone: $\sigma_i = \frac{\sigma_{\theta i}}{2\pi}\frac{c}{f_i}\frac{1}{2}$

From Phase lock loop theory: $\sigma_{\theta i} = 1/\sqrt{2SNR_i}$

Under shot noise limit: $SNR_i = \dfrac{\frac{1}{2}\left(\frac{\eta}{hf}\bar{P}_r\alpha m_i\right)^2}{\left(\frac{\eta}{hf}\bar{P}_r\right)2BW_i} = \frac{1}{4}\cdot\frac{\alpha^2 m_i^{\,2}}{BW_i}\left(\frac{\eta}{hf}\bar{P}_r\right)$

and $\sigma_i = \dfrac{c}{2\sqrt{2}\pi f_i}\cdot\dfrac{1}{\alpha m_i}\cdot\dfrac{1}{\sqrt{\frac{\eta}{hf}\frac{\bar{P}_r}{BW_i}}}$

For Example (GAMES):

Use 4 tones with the fourth for fine ranging (f_4=2 GHz)

m_4=090, m_0=m_1=m_2=0.1/3, α=0.85,

R_{max}=200 km, BW=1 Hz, $\frac{\eta}{hf}\bar{P}_r$=5x10^6 photons/sec

SNR = 1125 (30.5 dB),

σ_θ=0.021 rad,

$\frac{f_i}{f_{i-1}}$ = 74.5 for the first three tones

f_0=c/2R_{max}=750 Hz

f_1 = 55 kHz

f_2 = 4.1 MHz

f_4= 2.0 GHz

Space Radiation Effects on Photodetectors for GAMES and GLAS

Xiaoli Sun/JHU (rev. 2, Nov. 1993)

SUMMARY

GAMES and GLAS are expected to have a total radiation doses of 5 krad and 10 krad, respectively, with 100 mil thickness aluminum shielding, and 2 krad and 4 krad with 200 mil shielding. The peak dose rates are about 10^{-3} rad/s with 100-200 mil shielding. The principle radiation particles are protons and electrons in the South Atlantic Anomaly (SAA) region and the cosmic rays near the two horns at the poles of the magnetosphere. The electron radiation can be attenuated to a negligible amount after 7 mm Al shielding. The radiations of concern are the trapped protons in SAA and solar protons.

The PMT in GAMES is expected to suffer little long term damage after 10 krad dose. The transient radiation induced noise counts are estimated to be $2 \cdot 10^4$/s and $8 \cdot 10^5$/s for a rad-hard and a non rad-hard PMT, respectively, which is not likely to cause significant degradation in the overall receiver performance since the dark counts due to stray light still dominates. However, radiation damages to the GaAs photocathods and microchannel plates still need to be studied.

Si CCDs are inherently soft to radiation damages. The most significant damages are the reduction in the charge transfer efficiency and increases in the dark current due to surface ionization damages and bulk crystal lattice displacements. Some CCDs start to show noticeable performance degradation after less than 1 krad. Consequently, ordinary Si CCDs may not meet the requirement for GAMES, and therefore, rad-hard CCDs, such the CCDs in star trackers, should be used.

Si APDs for GLAS may experience more than an order of magnitude increase in bulk leakage current, up to 720 pA for the 1.064 μm wavelength enhanced APD and 60 pA for the 600 nm wavelength Geiger mode Si APD, after a total proton dose of 4 krad. The 1.064 μm altimeter receiver performance will be affected somewhat but the Geiger mode APD in the lidar receiver is expected to suffer series performance degradation due to the increase in dark counts, $>10^6$/s at the end of the five year mission.

I. Space Radiation Environment for GAMES and GLAS Spacecraft

A. South Atlantic Anomaly (SAA), near 30° S. Latitude/345° E. Longitude (Messenger (1992), ch. 8), (Stassinopoulos (1988)). Mostly protons of energy 0.1-5 MeV and electrons of energy < 2 MeV.

B. Cosmic Rays and solar flare protons near the two geomagnetic polar regions (the two horns at the poles of the magnetosphere). (Messenger, Stassinopoulos (1988), Barth).

C. The total expected space radiation exposure for GAMES and GLAS missions are 5 krad/4yrs and 10 Krad/5yrs, respectively, with 100 mils thickness shielding and 2 Krad/4yrs and 4 Krad/5yrs with 200 mils shielding. The total dose decreases very slowly as the shielding thickness increases to beyond 1/4 inch (500 mil). The peak dose rates are well below 10^{-3} rad/s with greater than 100 mil shielding. The details are given by Barth and Stassinopoulos (1993a, 1993b).

D. A review of radiation testing of semiconductor devices for space electronics has been given by R. L. Pease et al (1988).

E. A general theory of radiation damages to microelectronics devices including opto-electronics devices have been given by Srour (1988) and Messenger (1992).

II. Radiation Effects on PMT for GAMES

A. Transient Effects

1. Scintillation and fluorescence of the glass window, causing the dark current to increase proportionally to the radiation dose rate up to 10^{10} rad/hr with recovery time of up to 30 μs (Johnson, Viehmann, Levy).

2. Cerenkov emission, photons emitted by electrons traveling faster than light in glass (Birnbaum). Most of the Cerenkov electrons may be baffled out because they travel in specific direction and last only for picoseconds. The noise due to this effect appears as huge but short current spike at the PMT output and therefore can often be discriminated

3. Secondary electron emission of the window material.

4. Direct bombardments of electron radiation on the dynodes.

5. Bremsstrahlung photons (photons released by the electrons decelerated in the shield).

B. Long Term Damage

1. No long term damage under low dosage (10^4 rads) (Johnson).

2. Fluorescent and phosphorescence, lasting for days, weeks, and sometimes even months (Viehmann), causing the PMT dark current to increase by a few orders of magnitude (e.g. increased by about a factor of 10 after 10^5 rad (Johnson)).

3. Minor changes in photocathod quantum efficiency (Johnson).

4. Window brownish and higher transmission loss (Johnson).

5. The photocathod itself suffers little damage because it is thin and has a low absorption coefficient to high energy particles. The damage to the dynode chain can also be neglected (Johnson).

6. The radiation effects on PMTs are almost independent of the temperature (Johnson).

C. Radiation Hardness, Shielding and Protection

1. Minimizing the size and the thickness of the glass window.

2. Proper choice of the window material (Johnson, Viehmann, and Birnbaum).

3. Minimizing the size of the photocathod to reduce the collection area of radiation induced photons.

4. Electron focusing and baffling (Birnbaum).

5. Anode current limiting to prevent burn-out by transit effect.

6. Turning off the power at the peak of the radiation.

7. Shielding with Aluminum, 6 mm thick would stop almost all the electrons and reduces the protons flux by more than one order of magnitude (Viehmann). More detailed data on shielding are given by Barth and Stassinopoulos.

8. Very high energy particles and cosmic gamma rays cannot be shielded with reasonable amount of aluminum (Rasmussen). However, their occurrences are rare and only cause single event phenomena which is not a primary concern for GAMES and GLAS.

D. Some Test Results of PMT for Galileo (Birnbaum et al (EMR))

1. Use of ^{60}Co Gamma Ray as test source which induces equal amount of florescence.

2. The PMT is space qualified for the Galileo mission around Jupiter which has a harsher radiation environment than earth.

3. The rad-hard PMT produced about 2 times 10^7 counts/s per rad/s, roughly 2.5% the noise count by a conventional 1" diameter PMT.

E. Expected Radiation Damage to the GAMES PMT

1. The radiation induced noise counts should be well below the estimated noise count due to stray light (10^6/s).

2. The EMR PMT produce 10^6/s noise counts at about 0.4 rad(Si)/s.

3. The peak dose rate likely to be encountered by GAMES is well below 10^{-3} rad(Si)/s with 100-200 mil shield according to Barth and Stassinopoulos (1993a, Fig. 25-27). The expected noise counts

due to radiation is therefore less than 20,000/s and 800,000/s for the EMR rad hard PMT and conventional PMTs, respectively.

4. The GAMES receiver should be able to tolerate a long term dark count increase by more than a factor of 10 (a total dose of 10^5 rad according to Johnson).

5. The GAMES PMT should suffer little radiation damage, even with non rad-hard PMT provided it is shielded with more than 100 mils thick aluminum.

F. New Issues to be Studied about Radiation Effect on GAMES PMT

1. No test data was found on GaAs photocathods which are believed to be more sensitive to radiation damage.

2. No test data was found about multichannel plates.

3. There may be some test data about GaAs photocathod night vision instrument.

III. Radiation Effects on CCDs for GAMES

A. Transient Effects

1. Increasing noise counts due to ionization radiation, e.g. at $4.3\times10^{13}/cm^3$ new hole-electron pairs per rad(Si) (Killiany, p. 158).

2. The statistics of the dark counts generally do not follow Poison distribution and have a much larger standard deviation (e.g. 30 times for 1.25 MeV gamma rays) as compared with that of a Poison random variable (Killiany, p. 161).

3. Well saturation, blooming into adjacent pixels, or even burn-out due to noise photocurrent spikes. Well saturations occur for dose rate less than 1.0 rad per pixel integration time (Killiany). The recovery time depends on the clock rate and may be as long as milliseconds (Killiany, p.159).

4. Single event phenomena, i.e. single pixel saturation or burn-out.

B. Long Term Damages

1. Ionization damages. Protons and electrons from the radiation create electron-hole pairs within the insulation silicon oxide under the gate, as in a MOSFET. Because of the different mobilities, electrons are swept away and holes left behind, causing a positive charge build up in the oxide. Radiation also causes increases in the interface state density (traps formed due to crystal lattice discontinuity between silicon channel and the gate oxide) (Messenger, p. 281) (Killiany, p. 156).

a. Flat band (threshold) voltage shift

1) 0.3 V/krad as reported by Roy (1989), 0.09 V/krad by Hopkinson (1991, 1992). About 0.01V/krad for electron bombardment, as reported by Roy.

2) There were no significant annealing effect on flat band shift (Hopkinson (1991, 1992)).

3) The flat band voltage shift is much larger for positive gate than for negative gate voltages (n channel), because the charges are trapped near the gate oxide interface in the later case.

4) The flat band voltage shift is larger at lower temperature due to the longer trap life time.

5) The flat band shift was shown to be 3-4 times smaller if the devices were not powered (Hopkinson (1992)).

6) Uniform flat band voltage shift up to a few voltages may be compensated by increasing the reset voltage. Non-uniformities in flat band voltage shift form traps and cause signal distortion (Killiany).

b. Charge transfer efficiency (CTE) decrease due to radiation induced interface state density increase. The CCD read noise will increases as CTE decreases.

1) Charge transfer inefficiency (CTI=1-CTE) increased from 6×10^{-6} to 3×10^{-5} after 340 rads of 6.5 MeV protons, from 10^{-5} to 8×10^{-4} for high resistance devices after 2 krad of 10 MeV protons with little temperature dependence (Abbey).

2) CTI dropped to twice the pre irradiation level after 16 hr 140°C annealing (Abbey).

3) CTI becomes too high for the CCD to operate after 10^5 rad for most of the applications (Killiany).

4) Normal operation requires $CTI\times N<<0.1$ where N is the number of charge transfers (number of pixels in a column plus the number of shift register stages).

5) Interface state trapping effects are much less for buried channel CCDs than for surface channel CCDs.

c. Surface dark current increase due to interface state density increase (GAMES tracking CCD requires $I_{dark}<<10$ nA/cm^2).

1) Dark current increase at 10 nA/cm^2/Krad as reported by Hopkinson (1991, 1992).

2) Pixel to pixel dark current non-uniformity was not significant (Hopkinson (1991)).

3) The increase in dark current was about factor 2-4 less when the devices were not biased.

4) The dark current increased by 12 nA/cm^2 after 100 krads of electron radiation (Roy).

5) The dark current continued to increase after the radiation, the final dark currents became 2-3 times those immediately after

the radiation (Hopkinson (1991, 1992)). This antiannealing effect was not well understood and did not always occur (e.g. Abbey).

6) The dark current decreased with temperature (Hopkinson (1992), Roy).

d. A well designed CCD readout circuit suffered little radiation damage as compared with other parts of the CCD (Killiany).

e. The power consumption of the CCD increased slightly with radiation dose (e.g. 0.04 to 0.2 mA/rad) (Hopkinson (1991)).

f. It is widely assumed that equal doses of gamma rays and protons result in similar amounts of ionization damages, regardless of the proton energy (Raymond). Gamma rays are often used as test radiation sources.

2. Crystal lattice displacement upon impacts by protons, forming defects which act as traps and charge recombination centers (Killiany, Hopkinson (1991, 1992)). However, the principle damages of CCDs due to protons and electrons are ionization damages.

a. Dark current increases, 2.4 $nA/cm^2/MeV$ 3 months after 3 krads proton dose, with negligible pixel to pixel variation. Dark current due to bulk damage annealed after storage at room temperature (Hopkinson (1992,1992)).

b. Charge transfer efficiency may decrease due to traps. The effects depend on the bulk trap emission time constant (0.53 ms as reported by Killiany) and the clock frequency.

c. Degradation of minority carrier life time and concentration (no direct effect on imaging sensors but on the readout circuit.

d. Protons only cause minor bulk displacement damages (which are the principle damages by neutrons). A dose of 1 rads protons of

1-100 MeV is equivalent to 1-2 times 10^7 n/cm^2 1 MeV neutron fluence (Raymond).

e. The displacement damages due to protons starts to cause noticeable performance degradation at greater than 10 krads (about 10^{11} n/cm^2 equivalent neutron fluence) (Killiany, p. 163).

f. Displacement damage affects buried channel CCDs more than surface CCDs.

g. Displacement damages due to Gamma rays are insignificant for dose less than 10^6 rads(Si) (Killiany).

C. CCD Radiation Hardness

1. Aluminum shielding, 3 gm/cm^2 stops most of the electrons and reduces the protons flux by more than one order of magnitude (Stassinopoulos).

2. Use of buried n-channel devices.

3. Keep high uniformity across the entire imaging sensor array.

4. Use of a threshold voltage tracker.

5. Proper choice of the gate oxide.

6. Turning off the power during the peak of radiation

7 Current limiting to prevent pixel burn-out.

8. Software correction or fault tolerance. Radiation induced noisy pixels appear scattered and instantaneous while the tracking beacon moves relatively slowly in a somewhat predictable way.

9. In general, Si CCDs have initial observed degradation with potential failure after 10^4 rads, and severe degradation with high probability of total failure after 10^5 rads (Messenger, p. 642).

10. Modern rad-hard CCDs can be almost immune to ionization damage and its performance is primarily limited by the displacement damages (Dale et al).

D. Expected Radiation Damage on the GAMES CCD Tracking Detector

1. Transient effects: About 2,600 hole-electrons will be generated in a 20 by 20 by 15 μm^3 pixel per frame (0.1 seconds) at the peak of the radiation dose rate (10^{-3} rad/s).

2. Flat band shift: < 0.1 V/Krad ×10 Krad = 1.0V, which can be easily accommodated.

3. Charge transfer inefficiency increases: CTI may drop from 10^{-5} to 8×10^{-4} after 2 Krad, which is unacceptable.

4. Dark current increases: 10nA/cm^2/Krad × 4 = 40 nA/cm^2, which is also unacceptable.

5. The above results may be over pessimistic since most of the numbers quoted were drawn under the worst cases. Characteristics of radiation damages vary widely from devices to devices. A new test should be conducted for the GAMES CCD.

6. The GAMES CCD and its shield have to be carefully designed or it will not meet the mission requirements. The primary damages are the increases in charge transfer efficiency and dark current due to ionization (0.5" shielding may have to be used to keep the radiation dose inside the shield well below 1 Krad).

III Radiation Effects on Si APDs for GLAS

A. Transient Effects

1. Shot noise due to the radiation induced photocurrent, $I_{rp}= q\cdot g_0\cdot(G\cdot V_G + V_s)\cdot(d\gamma/dt)$ with q the electron charge, g_0 the charge generation rate ($4.04\cdot10^{13}$ /rad/cm^3), G the average APD gain, V_G the volume of the APD high field region, V_s the volume of the APD which contribute to surface current, and $d\gamma/dt$ (rad/s)

the dose rate. For example, I_{rp}=175 nA and I_{rp}=156 nA under 28 rad/s ^{60}Co gamma ray and 1.5 MeV electron radiation for a EG&G C30902S Si APD at G=100 (Swanson).

2. Noise generation at the glass window, as in PMTs.

B. Long Term Damages

1. Increase in bulk leakage current due to displacement damages to the crystal lattice, at $\Delta I_{bulk}=\alpha\cdot\phi\cdot V$, with α the leakage current constant, ϕ the neutron radiation fluence, and V the volume of the active region of the APD (Kraner).

a. Since 1 rad 1-100 MeV protons causes the same amount displacement damage as about $1.5\cdot10^7$/cm^2 1 Mev neutron fluence (Raymond), $\Delta I_{bulk}=\alpha\cdot1.5\cdot10^7\cdot V$ (A/rad).

b. Geiger mode Si APD (10V above the breakdown point), $\alpha=1.7\cdot10^{-16}$ A/cm (EG&G C30902S, V=$6\cdot10^{-6}$ cm^3) (Buchinger), therefore, ΔI_{bulk}=15 pA/krad.

c. Analog mode Si APD (EG&G C30902S), I_{bulk} increased from 0.01 pA to 3 pA after 200 Krad 1.5 Mev electron radiation (Swanson). However, the increase in I_{bulk} due to protons of the same dose should be several orders of magnitude greater (Van Lint, 1975).

d. For the Si APD used in MOLA, d=800μm, L=140μm (Hammond), V=$7.032\cdot10^{-5}$ cm^3, ΔI_{bulk}=180 pA/krad for proton radiations.

2. Increase in surface leakage current, primarily due to ionization damages at the APD surface between the insulation layer and the bulk (Swanson).

a. The increases in I_S should follow about the same rule as for Si MOSFET, in the order of 10 nA/cm^2/krad.

b. The surface leakage currents are known to exhibit 1/f noise (Swanson).

c. The noise due to surface leakage current is usually much smaller than other noise sources, e.g. bulk leakage current and preamplifier noise).

3. Decreases in quantum efficiency due to surface leakage and carrier lifetime reduction due to radiations (Kalma, Wiczer, Barnes). However, this effect may be minimized by using a smaller load resistor for the photodiode.

a. A reduction of quantum efficiency of 15% and 65% were observed after 10^5 and 10^8 rad for Si PIN photodiode (Kalma).

b. The lifetime reduction due to radiation displacement damage only affects low frequency response (Kalma).

4. Damages to the preamplifier. GaAs preamplifiers use MESFET (JFET) and therefore are much more resistant to ionization radiation damages than Si MOSFET devices (Messenger).

C. Photodiode Radiation Hardness

1. APDs are much more sensitive to radiation damages than PIN photodiodes because ΔI_{bulk} is multiplied by the APD gain. Unlike PIN photodiodes, the APD dark noise is usually comparable with the preamplifier noise, and therefore, the increase in the APD dark current due to radiation are much likely to degradation in the receiver performance.

2. The window material has to be chosen with care, as for PMTs.

3. It is recommended that the shielding for the APD be increased to 0.5" so that the net dose at the APD is below 1 krad for the GLAS mission. However, further increasing the shielding should have little effect in reducing the total dose (0.6 krad after 1.5").

4. Several rad-hard photodiode structures have been published (Wiczer, Barnes), but they may not be needed for the GLAS mission.

5. Si APDs were known to have passed radiation tests for free space laser communications, up to 10^5 rad. However those are all gamma ray tests done at EG&G (according to my conversation with Dr. McIntyre). Protons of the same dose are expected to cause much more long term damages to the APDs.

D. Expected Radiation Damage to the Si APD in GLAS

1. Total transient bulk dark current increase by about 0.056 pA under the expected 10^{-3} rad/s peak dose rate, which is well below the average APD bulk dark current in analog mode.

2. The transient increase in the noise counts in a Geiger mode APD for the lidar will be less than 0.056pA/q =355,000 counts/sec, which should not cause device saturation. detection prob.

3. Permanent bulk dark current increase by about 0.72 nA and 60 pA for the 1 μm enhanced Si APD and the Geiger mode APD for the lidar, respectively, after 4 krad total dose over the entire 5 years GLAS mission (200 mil shielding).

4. The increase in bulk leakage current will cause the APD dark noise spectral density to rise to a few times the preamplifier noise (2 $pA/Hz^{1/2}$) at the end of the mission, which will cause some but not catastrophic performance degradation.

5. The radiation induced noise counts in Geiger mode APD in the lidar would greatly exceed the saturation level (10^7 counts/s) at the end of the mission regardless of the shielding thickness.

6. Little loss in quantum efficiency at the end of the mission (4 krad total dose).

7. The effect of increase in bulk leakage current on receiver performance is far more severe for APDs than for PIN photodiodes. The former is usually operated close to shot noise regime and the latter operated in preamplifier noise limited regime.

E. Some Radiation Test Data of the APDs for Laser Com and MOLA

1. EG&G C30902E APD and preamp module by TRW was reported to have passed 10^5 rad(Si) gamma rays with no damage except a 30% increase in the dark current (Conner).

2. The specification of the APD for MOLA by McDonald Douglas said that the APD shall not be permanently damaged and shall perform within the specified limits after 10^5 rad(Si) of radiation.

3. The radiation dose should be assumed as the dose outside of the package. The APD itself inside the shield may have experienced less than 10^4 rad.

F. New Issues to be Studied

1. There has been no measurement data on long term damages due to proton radiations. Protons, which are the primary radiation in the GLAS orbit, are expected to cause significant increase in I_{bulk} due to displacement damages. Dr. McIntyre who is the leading expert in the field of APDs also expressed concerns about proton damages to Geiger mode APDs.

2. It is recommended that we do a proton radiation test on Si APDs, especially Geiger mode APD photon counter.

References

Abbey, A., A. Holland, D. Lumb, and K. McCarthy, "Further proton damage effects in EEV CCDs," in *Proceedings ESA Electronic Components Conference, ESTEC*, Noordwijk, The Netherlands, Nov. 12-16, 1990, ESA SP-313, pp. 307-317.

Aukerman, L. W., F. L. Vernon, Jr., and Y. Song, "Radiation threshold levels for noise degradation of photodiodes," *Optical Engineering*, Vol. 23, No. 5, pp. 678-684, Oct. 1984.

Barnes, C. E., "Radiation Effects on light sources and detectors," *Radiation Effects in Optical Materials*, P. W. Levy, editor, SPIE Proceedings, Vol. 541, pp. 138-149, March 6-7, 1985, Albuquerque, New Mexico.

Barth, J. L., E. G. Stassinopoulos, *Space Radiation Exposure of the GLAS Mission*, X-900-93-06, NASA-Goddard Space Flight Center, Radiation Physics Office, Earth Sciences Directorate, August 1993.

Barth, J. L., E. G. Stassinopoulos, *Space Radiation Exposure of the GAMES Mission*, X-900-93-07, NASA-Goddard Space Flight Center, Radiation Physics Office, Earth Sciences Directorate, August 1993.

Birnbaum, M. M., R. L. Bunker, J. Roderick, and K. Stephenson, "Development of a radiation-hard photomultiplier tube," *AIAA Guidance and Control Conference (AIAA'84)*, Seattle, WA, Aug. 20-22, 1984 (AIAA-84-1852).

Buchinger, F., H. Dautet, J. K. P. Lee, R. J. McIntyre, and M. Orchard-Webb, "Real-time monitoring of single-neutron-induced damage in silicon using avalanche photodiode operating in the Geiger mode," *Nuclear Instruments and Methods in Physics Research*, Vol. B72, pp. 496-498, 1992.

Conner, J. L. and J. L. Guggenmos, "Direct detection avalanche photodiode receiver design for the NASA/DDLT," *Optomechanical Design of Laser Transmitters and Receivers*, SPIE vol. 1044, pp. 145-154, 1989.

Dale, C., P. Marshall, B. Cummings, L. Shamey, R. Howard, and A. Delamere, "Spacecraft displacement damage dose calculations for shielded CCDs," *High-Resolution Sensors and Hybrid Systems, SPIE proceedings*, vol. 1656, 1992.

Hammond, S. D., "Improved avalanche photodiode and hybrid preamplifier for 1064 nm wavelength, *Free-space laser communication technologies II*, SPIE Proceedings, Vol. 1218, pp. 635-643, 1990.

Hopkinson, G. R., "Space radiation effects on CCDs," in *Proceedings ESA Electronic Components Conference, ESTEC*, Noordwijk, The Netherlands, Nov. 12-16, 1990, ESA SP-313, pp. 301-306.

Hopkinson, G. R., "Radiation Effects on CCDs for spaceborne acquisition and tracking applications," *First European Conference on Radiation and its Effects on Devices and Systems, RADECS'91*, La Grande-Motte, France, Sept. 9-12, 1991, pp. 368-372 (published by IEEE).

Johnson, S. M., "Radiation effects on multiplier phototubes," *IEEE Trans. Nucl. Sci.*, Vol. NS-20, No. 1, pp. 113-124, Feb. 1973.

Kalma, A. H. and W. H. Hardwick, "Radiation testing of PIN photodiodes," *IEEE Trans. Nuclear Science*, Vol. NS-25, No. 6, pp. 1483-1488, Dec. 1978.

Killiany, J. M., "Radiation effects in silicon charge-coupled devices," in *Charge-Coupled Devices*, D. F. Barbe, editor, Springer-Verlag, New York, 1980, ch. 6.

Kraner, H. W., and Z. Li, "Fast neutron damage in silicon detectors," *Nuclear Instruments and Methods in Physics Research*, Vol. A279, pp. 266-271, 1989.

Levy, P. W., "Overview of nuclear radiation damage processes: phenomenological features of radiation damage in crystals and glasses," Radiation Effects in Optical Materials, *Radiation Effects in Optical Materials*, P. W. Levy, editor, SPIE Proceedings, Vol. 541, pp. 2-24, March 6-7, 1985, Albuquerque, New Mexico.

Messenger, G. C. and S. A. Ash, *The Effects of Radiation on Electronic Systems*, New York: Van Nostrand Reinhold, 2nd ed., 1992.

Pease, R. L., A. H. Johnston, and J. L. Azarewicz, "Radiation testing of semiconductor devices for space electronics," Proceedings of IEEE, Vol. 76, No. 11, pp. 1510-1526, Nov. 1988.

Rasmussen, R. D., "Spacecraft electronics design for radiation tolerance," Proceedings of IEEE, Vol. 76, No. 11, pp. 1527-1537, Nov. 1988.

Raymond, J. P. and E. L. Petersen, "Comparison of neutron, proton and gamma ray effects in semiconductor devices," *IEEE Trans. Nuclear Science*, Vol. NS-34, No. 6, pp. 1622-1628, Dec. 1987.

Roy, T., S. J. Watts, and D. Wright, "Radiation damage effects on imaging charge coupled devices," *Nuclear Instruments and Methods in Physics Research*, Vol. A275, pp. 545-557, 1989.

Srour, J. R., and J. M. McGarrity, "Radiation effects on microelectronics in space," *Proceedings of the IEEE*,, Vol. 76, No. 11, pp. 1443-1469, Nov. 1988.

Stassinopoulos, E. G. and J. P. Raymond, "The space radiation environment for electronics," *Proceedings of the IEEE*, Vol. 76, No. 11, pp. 1423-1442, Nov. 1988.

Swanson, E. A., Elaine R. Arnau, and F. G. Walther, "Measurements of natural radiation effects in a low noise avalanche photodiode," *IEEE Trans. Nuclear Science*, Vol. NS-34, No. 6, pp. 1658-1661, Dec. 1987.

Van Lint, V. A. J., C. Gigas, and J. Barengoltz, "Correlation of displacement effects produced by electrons protons and neutrons in silicon," IEEE Trans. Nuclear Science, Vol. NS-22, No. 6, pp. 1663-2668, Dec. 1975.

Viehmann, W., A. G. Eubanks, G. F. Pieper, and J. H. Bredekamp, "Photomultiplier window materials under electron irradiation: fluorescence and phosphorescence," *Applied Optics*, Vol. 14, No. 9, pp. 2104-2115, Sept. 1975.

Wiczer, J. J., "Radiation-hardened optoelectronics components: detectors," *Optical Technologies for Communication Satellite Applications*, K. Bhasin, editor, SPIE Proceedings, Vol. 616, pp. 254-266, Jan. 21-22, 1986, LA, CA.

Receiver Performance Analysis of the GAMES PN Code Coarse Ranging Subsystem

Xiaoli Sun
Dept. ECE, The Johns Hopkins University
December 1993

1. Design of the GAMES PN Code Coarse Ranging Subsystem

Figure 1 shows a block diagram of the GAMES coarse ranging subsystem design. The laser diode transmitter is modulated by both a sinusoidal signal as the subcarrier and a pseudo noise (PN) binary sequence as the subcarrier amplitude modulation. The former is for the fine ranging and the latter is for the coarse ranging. Figure 2 shows the two possible combinations of these two modulation signals along with the hardware of how to realized them. Both of those modulation formats should result in the same coarse ranging performance. The depth of the PN code subcarrier modulation is no greater than 10%.

Norman and Gardner [1] have shown that the optimal detection scheme for a PN code ranging system is the cross-correlation of the received photon counts with the PN code to find the maximum. One can also average the correlator output over a number of PN code period to improve the signal to noise ratio (SNR). To reduce the required computer time, one can equivalently form a histogram of the detected photon counts over a number of code periods and then cross correlate the histogram with the PN code, as shown in

Figure 1. The cross correlation and the peak detection can be done in software.

2. Coarse Ranging Performance

2.1. The Ranging Resolution

The resolution of the coarse ranging subsystem, Δd, is given by

$$\Delta d = c/2\tau_{bin} \quad (1)$$

where c is the speed of light and τ_{bin} is the duration of each bin of the histogrammer. The value of τ_{bin} is usually equal to the bit time of the PN code. There may well be misalignment between the histogrammer and the received PN code. The largest timing offset is $\tau_{bin}/2$. This timing misalignment causes the peak value of the correlator output to decrease by as much as a factor of two for rectangular PN code pulse shapes. The amount of the noise of the correlator output is not affected.

2.2. SNR at the Output of the Correlator

The other important criterion of the ranging performance is the false alarm probability in locating the correlation peak. Because the low PN code modulation depth (sometimes called modulation index), the dominate noise source for the coarse ranging subsystem is the stray light and the unmodulated fine ranging signal. The statistics of the total noise in the correlator output can be assumed to follow the Gaussian distribution. The false alarm probability under this

assumption is solely determined by the SNR of the correlator output and the PN code length.

The average detected photon counting rate can be written as

$$\lambda(t,T_d)=\frac{\eta}{hf}[(1-m_{PN})L_pP_s+P_b] + \frac{\eta}{hf}[m_{PN}L_pP_s\sum_{i=-\infty}^{\infty} a_ip(t-i\tau-T_d)] \quad (2)$$

where η is the photodetector quantum efficiency, hf is the photon energy, m_{PN} is the modulation index, L_p is the total signal round trip propagation loss, P_s is the transmitted optical power averaged over a bit time, P_b is the background noise power, a_i=0,1 is PN code, p(t) is the transmitted laser pulse shape, τ is the PN code bit time, and T_d is the time delay due to light propagation. The laser pulse shape is assumed to be a rectangle of unity amplitude and one bit time duration.

The photodetector output is a Poisson random point process with the counting rate given by (2). The histogrammer output can be written as a random sequence, $x_0, x_1,\ldots,x_{N-1}$, with each element equal to the number of photons collected in that bin. It can be shown [2] that $x_0, x_1,\ldots,x_{N-1}$ are independent Poisson random variables with mean given by

$$\bar{x}_k=M\times\lambda(k\tau,T_d)\tau=M\frac{\eta}{hf}m_{PN}L_pP_s\tau\, a_{k+l} + M\frac{\eta}{hf}[(1-m_{PN})L_pP_s+P_b]\tau \quad (3)$$

where M is the number of PN code periods which the histogrammer has integrated and the propagation delay time, T_d, is assumed to be equal to integer number of bit time, i.e. $T_d=l\tau$.

The signal output from the correlator can be written as

$$y_j = \sum_{i=0}^{N-1} x_i a'_{i+j} \tag{4}$$

where

$$a'_i = 2a_i - 1 \tag{5}$$

is the bipolar form of the PN code.

Since the histogrammer output $x_0, x_1,\ldots,x_{N-1}$ are independent Poisson random variables, the mean of the correlator output can be derived as

$$\sum_{i=0}^{N-1} \bar{x}_i a'_{i+j}$$

$$= M\frac{\eta}{hf} m_{PN} L_p P_s \tau \sum_{i=0}^{N-1} a_{k+l} a'_{i+j} + M\frac{\eta}{hf}[(1-m_{PN})L_p P_s + P_b]\tau \sum_{i=0}^{N-1} a'_{i+j} \tag{6}$$

When a maximum PN binary sequence of code length N is used, it has the following property

$$\sum_{i=0}^{N-1} a'_i = 1 \tag{7a}$$

and

$$\sum_{i=0}^{N-1} a_i a'_{i+j} = \begin{cases} \frac{N+1}{2}, & j = 0,1,2,\ldots \\ 0, & \text{else} \end{cases} \tag{7b}$$

The mean of the correlator output becomes

$$\bar{y}_j = \begin{cases} M\frac{\eta}{hf}[(1-m_{PN})L_p P_s + P_b]\tau + M\frac{\eta}{hf} m_{PN} L_p P_s \tau \cdot \frac{N+1}{2}, & j = l \\ M\frac{\eta}{hf}[(1-m_{PN})L_p P_s + P_b]\tau, & j \neq l \end{cases} \tag{8}$$

The useful signal is defined as peak value of the correlator output, $y_{j=l}$, minus the constant background, i.e.,

$$y_s = \frac{1}{2}M(N+1)\cdot\frac{\eta}{hf}m_{PN}L_pP_s\tau \tag{9}$$

The variance of the correlator output can be calculated as follows. Since the histogrammer output $x_0, x_1,...,x_{N-1}$ are independent Poisson random variables,

$$VAR\{y_j\} = \sum_{i=0}^{N-1}(a'_{i+j})^2\cdot VAR\{x_i\} = \sum_{i=0}^{N-1}VAR\{x_i\}\} = \sum_{i=0}^{N-1}\bar{x}_i \tag{10}$$

Substituting (3) into (10)

$$VAR\{y_j\} = M\frac{\eta}{hf}m_{PN}L_pP_s\tau\sum_{i=0}^{N-1}a_{i+l} + MN\frac{\eta}{hf}[(1-m_{PN})L_pP_s+P_b]\tau \tag{11}$$

Since $\sum_{i=0}^{N-1}a_i = \frac{N+1}{2}$,

$$VAR\{y_j\} = \sigma_y^2 = \frac{1}{2}M(N+1)\frac{\eta}{hf}m_{PN}L_pP_s\tau + MN\frac{\eta}{hf}[(1-m_{PN})L_pP_s+P_b]\tau \tag{12}$$

Notice that the variance is independent of the bin number.

A signal to noise ratio can be defined as

$$SNR = \frac{y_s}{\sigma_y} \tag{13}$$

Substituting (9) and (12) into (13)

$$SNR = \sqrt{\frac{M(N+1)}{2}} \cdot \frac{m_{PN}\frac{\eta\tau}{hf}L_p P_s}{\sqrt{m_{PN}\frac{\eta\tau}{hf}L_p P_s + \frac{2N}{N+1}\frac{\eta\tau}{hf}[(1-m_{PN})L_p P_s + P_b]}} \quad (14)$$

It is noticed that (14) is different from that given in [4] which we believe is incorrect.

If we define the average number of detected signal and background noise photons per bit time as

$$n_s = \frac{\eta\tau}{hf}L_p P_s \quad (15)$$

and

$$n_b = \frac{\eta\tau}{hf}P_b \quad (16)$$

the correlator output SNR becomes

$$SNR = \sqrt{\frac{M(N+1)}{2}} \cdot \frac{m_{PN} n_s}{\sqrt{m_{PN} n_s + \frac{2N}{N+1}[(1-m_{PN})n_s + n_b]}} \quad (17)$$

2.3. SNR for Non Photon Counting Receivers

The photodetectors, either a PMT or an APD, can operate in analog mode. The photodetector output in this case is simply the photocurrent integrated over a bit time. The receiver does not contain a discriminator but an integrator or a filter which perform the integration. Besides the shot noise associated with photon

detection, there is also the so called excess noise which results from the randomness of the photodetector gain. When an APD is used, the preamplifier noise also has to be considered.

The mean of the histogrammer output when an APD is used can be written similarly to Eq. (3), as

$$\bar{x}'_k = M\left[G\lambda(k\tau, T_d)\tau + G\frac{I_{db}\tau}{q} + \frac{I_{ds}\tau}{q}\right] =$$

$$= MG\frac{\eta_a}{hf}m_{PN}L_pP_s\tau\, a_{k+l} + MG\frac{\eta_a}{hf}[(1-m_{PN})L_pP_s+P_b]\tau + MG\frac{I_{db}\tau}{q} + M\frac{I_{ds}\tau}{q} \tag{18}$$

where G is the average photodetector multiplication gain, η_a is the quantum efficiency, and I_{ds} and I_{db} are the photodetector surface and bulk leakage current, and q is the electron charge. Notice that the quantum efficiency of an APD, η_a, is normally a few times photon counting probability in Geiger mode. The variance of the histogrammer output can be written as [5]

$$\mathrm{Var}\{x'_k\} = MG^2F\left[\frac{\eta_a}{hf}m_{PN}L_pP_s\tau\, a_{k+l} + \frac{\eta_a}{hf}[(1-m_{PN})L_pP_s+P_b]\tau + \frac{I_{db}\tau}{q}\right] + M\frac{I_{ds}\tau}{q} + M\frac{N_{amp}\tau}{2q^2} \tag{19}$$

where N_{amp} is the one sided spectral current density of the preamplifier noise in A^2/Hz and F is the APD excess noise factor given by [6]

$$F \approx k_{eff}G + (2-1/G)(1-k_{eff}) \tag{20}$$

with k_{eff} the effective APD hole to electron ionization coefficient ratio.

Substituting (18) and (19) into (6) and (10) and following the procedure given in the previous subsection, the correlator output SNR can be written as

$$SNR' = \sqrt{\frac{M(N+1)}{2}} \cdot \frac{m_{PN}\frac{\eta_a \tau}{hf} L_p P_s}{\left[F\frac{\eta_a \tau}{hf}[m_{PN}L_p P_s + \frac{2N}{N+1}[(1-m_{PN})L_p P_s + P_b] + F\frac{I_{db}\tau}{q}] + \frac{2N}{N+1}\frac{1}{G^2}(\frac{I_{ds}\tau}{q} + \frac{N_{amp}\tau}{2q^2})\right]^{\frac{1}{2}}} \quad (21)$$

or

$$SNR' = \sqrt{\frac{M(N+1)}{2}} \cdot \frac{m_{PN}n_s}{\sqrt{F\left[m_{PN}n_s + \frac{2N}{N+1}[(1-m_{PN})n_s + n_b + \frac{I_{db}\tau}{q}]\right] + \frac{2N}{N+1}\frac{1}{G^2}(\frac{I_{ds}\tau}{q} + \frac{N_{amp}\tau}{2q^2})}} \quad (22)$$

When a PMT is used, Eq. (22) can still be used to calculate the correlator output SNR provided an appropriate excess noise factor F (F=1.1-1.5) is used. The gain of a PMT is usually so large (>10^5) that the preamplifier noise can be ignored.

For base band PN code ranging system, there is no subcarrier. The laser diode is directly intensity modulated by the PN code. One can still use Eq. (17) and (22) to calculate the correlator output SNR

provided the modulation index, m_{PN}, is replaced by the laser OFF to ON extinction ratio.

2.4. Probability of Incorrect Measurement vs. SNR

The probability of the incorrect range measurement can be written as

$$P_E = \text{Prob}(y_l \le y_i,\ 0 \le i \le N-1,\ i \ne l) \tag{23}$$

As an approximation, we can assume that the y_i's follow the Gaussian distribution with the mean and variance given by (6) and (12). The probability of the incorrect range measurement can be written as

$$P_E = 1 - \int_{-\infty}^{\infty} \frac{1}{\sqrt{2\pi}\sigma_y} \exp\left[\frac{-(y_1-\bar{y}_l)^2}{2\sigma_y^2}\right] \left[\int_{-\infty}^{y_1} \frac{1}{\sqrt{2\pi}\sigma_y} \exp\left[\frac{-(y_2-\bar{y}_{i\ne l})^2}{2\sigma_y^2}\right] dy_2\right]^{N-1} dy_1 \tag{24}$$

or

$$P_E = 1 - \frac{1}{\sqrt{\pi}} \int_{-\infty}^{\infty} e^{-y^2} \left[1 - \frac{1}{2}\text{erfc}\left(y + \frac{SNR}{\sqrt{2}}\right)\right]^{N-1} \tag{25}$$

where erfc(x) is the complimentary error function defined as

$$\text{erfc}(x) = 1 - \text{erf}(x) = 1 - \int_0^x \frac{2}{\sqrt{\pi}} e^{-v^2} dv = \int_x^{\infty} \frac{2}{\sqrt{\pi}} e^{-v^2} dv \tag{26}$$

For large value of SNR,

$$P_E \approx \frac{N-1}{2\sqrt{\pi}} \int_{-\infty}^{\infty} e^{-y^2} \text{erfc}\left(y + \frac{SNR}{\sqrt{2}}\right) dy\ . \tag{27}$$

3. Numerical Results

The probability of ranging error was evaluated numerically using the software called Mathcad and the results are given in the attached computer printouts.

The first attachement shows the data and the plot of P_E vs. SNR for code length $N=2^9-1=511$. It shows that a SNR of 18 dB is required to achieve $P_E < 10^{-6}$ for N=511. This result can be scaled for other code lengths because P_E is proportional to the code length for any given SNR, as shown in (27).

The second attachement shows the calculated performance of the GAMES PN code coarse ranging sybsystem. A photon counting receiver is assumed. All the system parameter values used in the calculation are given in the printout. The total histogrammer integration time is taken to be 0.1 second. If we assume the target is moving at 1.0 m/s, the timing offset between of the histogrammer and the received PN code due to the Doppler shift will change by 2/3 ns (3.3% of the bit time) during the 0.1 second integration time interval. Furthermore, the SNR is reduced by one half in the calculation to account for the possible misalignment between origins of the histogrammer and the received PN code. The calculation results show that a detected signal photon rate of $1.9 \cdot 10^6$ is required to achieve $P_E < 10^{-6}$. The dominate noise sources are the shot noises from the signal and background light.

The third attachment is the same as the second but the laser modulation index was changed from 10% to 5%. A detected signal photon rate of $5.8 \cdot 10^6$ is required to achieve $P_E < 10^{-6}$ in this case.

The fourth attachement shows P_E vs. detected signal photons per bit time for a base band PN code ranging lidar system which use an APD photodetector in analog mode. The system parameter values used are typical for practical devices available today. The dominate noise source in this case is the preamplifier noise. The calculation results show that 2 photons/bit time is required to achieve $P_E < 10^{-6}$ for code length $N=2^7-1=127$.

For the same histogrammer integration time, the SNR at the correlator output is virtually independent of the code length according to Eq. (22). On the other hand, the ranging error probability is proportional to the code length for any given SNR. The code length should be determined by the maximum range the target or the minimum range unambiguity required by the system.

References

[1] D. M. Norman and C. S. Gardner, "Satellite laser ranging using pseudonoise code modulated laser diodes," *Applied Optics*, Vol. 27, No. 17, pp. 3650-3655, Sept. 1988.

[2] D. L. Snyder, *Random Point Processes*, John Wiley & Sons, New York, 1975, ch. 2.

[3] R. C. Dixon, *Spread Spectrum Systems*, John Wiley & Sons, New York, 1984, ch. 3.

[4] N. Takeuchi, H. Baba, K. Sakurai, and T. Ueno, "Diode-laser random-modulation cw lidar," *Applied Optics*, Vol. 25, No. 1, pp. 63-67, Jan. 1986.

[5] F. M. Davidson and X. Sun, "Gaussian approximation versus nearly exact performance analysis of optical communication systems with PPM signaling and APD receivers," *IEEE Trans. Commun.*, Vol. COM-36, No. 11, pp. 1185-1192, Nov. 1988.

[6] P. P. Webb, R. J. McIntyre, and J. Conradi, "Properties of avalanche photodiodes," *RCA Review*, Vol. 35, pp. 234-278, June 1974.

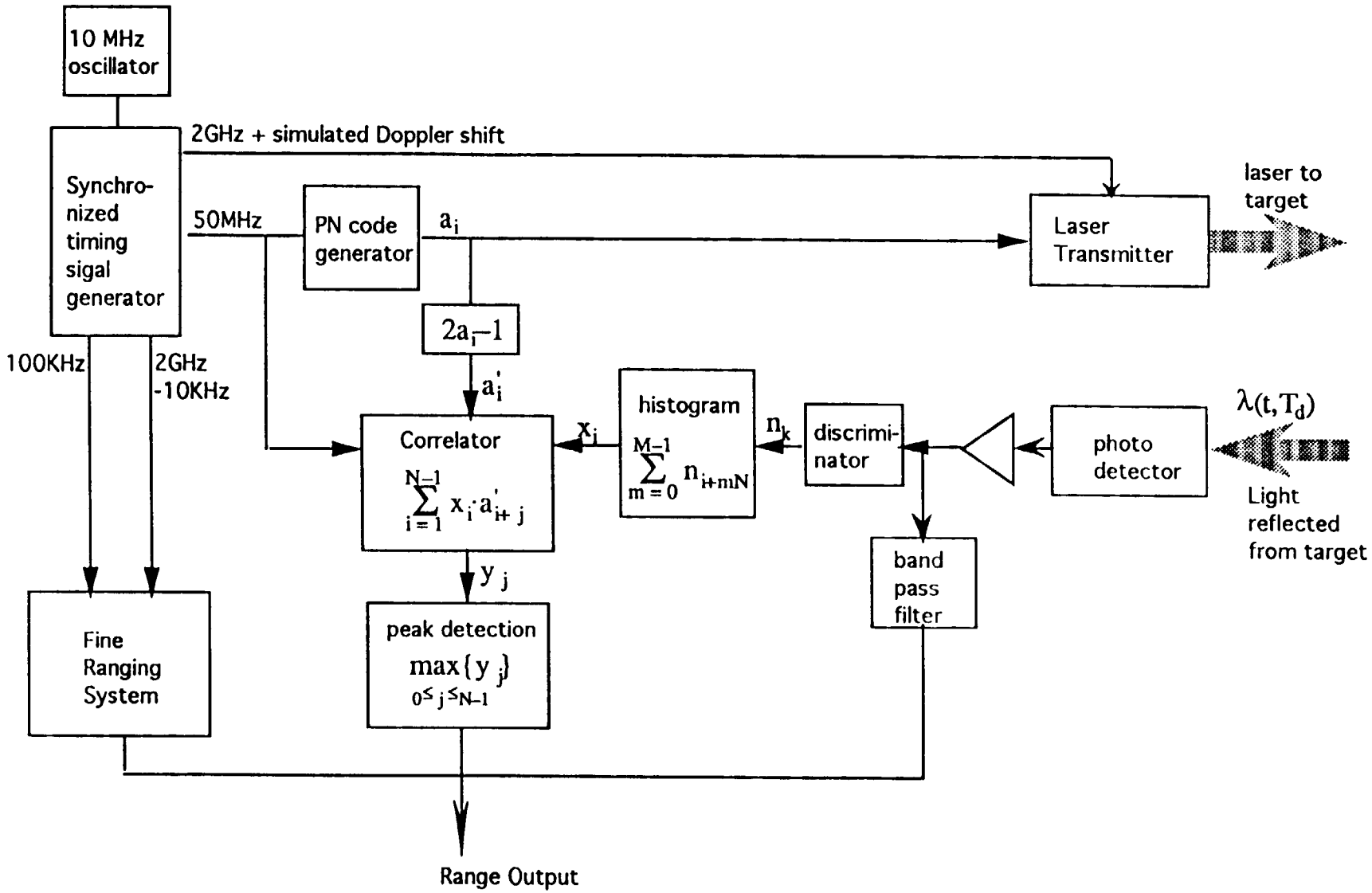

Figure 1. Design of the breadboard of the GAMES coarse ranging subsystm.

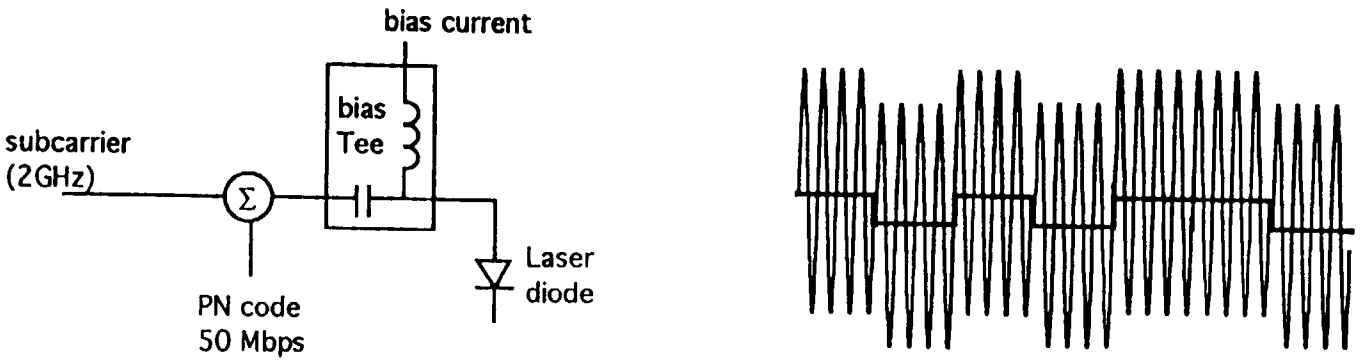

(a)

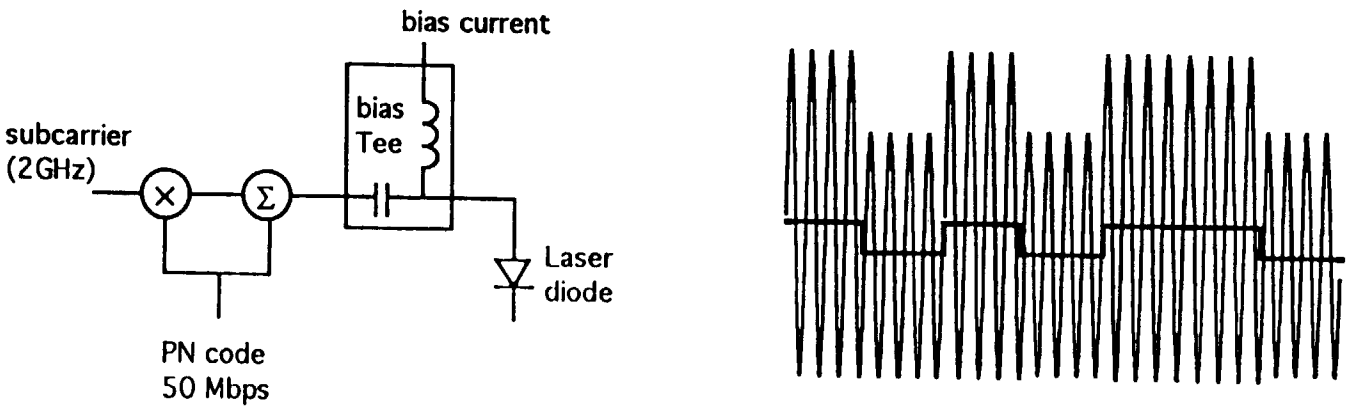

(b)

Figure 2. PN code subcarrier modulation for the GAMES coarse ranging subsystem.

Probability of Error vs. SNR of a PN Code Laser Ranging System

$N := 511$ The code length

$SNR := 5, 5.5 .. 15$

$$PE(SNR, N) := \frac{N-1}{2\cdot\sqrt{\pi}} \cdot \int_{-20}^{20} \exp(-y^2)\cdot\left(1 - \operatorname{erf}\left(y + \frac{SNR}{\sqrt{2}}\right)\right) dy$$

$TOL := 10^{-15}$ The integration tolerance

SNR	20·log(SNR)	PE(SNR, N)
5	13.979	0.1038
5.5	14.807	0.0257
6	15.563	$5.6331\cdot10^{-3}$
6.5	16.258	$1.0972\cdot10^{-3}$
7	16.902	$1.8949\cdot10^{-4}$
7.5	17.501	$2.9\cdot10^{-5}$
8	18.062	$3.9314\cdot10^{-6}$
8.5	18.588	$4.719\cdot10^{-7}$
9	19.085	$5.0137\cdot10^{-8}$
9.5	19.554	$4.7137\cdot10^{-9}$
10	20	$3.9205\cdot10^{-10}$
10.5	20.424	$2.8841\cdot10^{-11}$
11	20.828	$1.8762\cdot10^{-12}$
11.5	21.214	$1.3241\cdot10^{-13}$
12	21.584	$5.6189\cdot10^{-15}$
12.5	21.938	0
13	22.279	0
13.5	22.607	0
14	22.923	0
14.5	23.227	0
15	23.522	0

WRITEPRN(snrdat) := 20·log(SNR)

WRITEPRN(pedat) := PE(SNR, N)

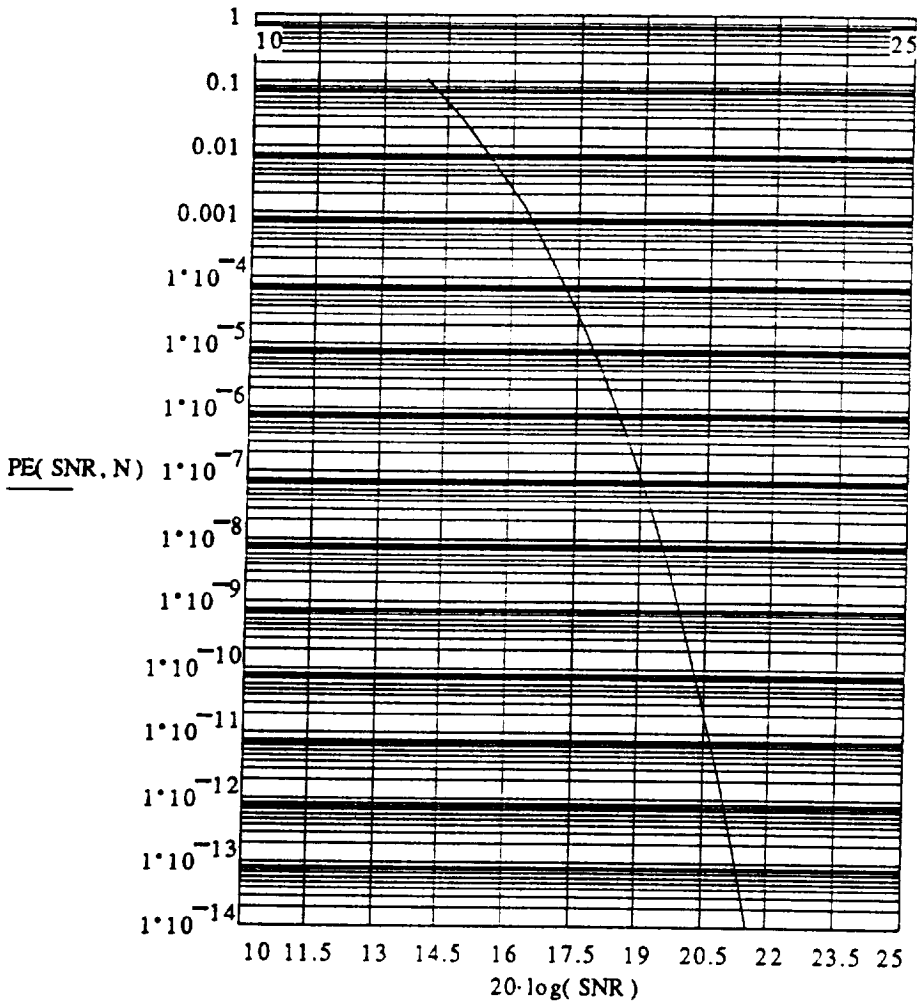
1
0.1
0.01
0.001
1·10^-4
1·10^-5
1·10^-6
1·10^-7
1·10^-8
1·10^-9
1·10^-10
1·10^-11
1·10^-12
1·10^-13
1·10^-14
PE(SNR, N)
10
25
10 11.5 13 14.5 16 17.5 19 20.5 22 23.5 25
20·log(SNR)

GAMES PN Code Coarse Ranging Subsystem Performance

PN CODE PARAMETERS

Code Length: $N := 2047$

Code bit rate (bps): $BR := 50 \cdot 10^6$

Bit time (second): $\tau := \frac{1}{BR}$ $\tau = 2 \cdot 10^{-8}$

Total Integration time of the histogrammer (second): $T := 0.1$

Number of code length averaged:

$$M := \text{floor}\left(\frac{T}{\tau \cdot N}\right) \qquad M = 2.442 \cdot 10^3$$

DETECTED SIGNAL AND NOISE PHOTONS

Detected signal photons per bit time:

$$n_s := 0.02, 0.0225 .. 0.05$$

Laser modulation index: $m_{PN} := 0.10$

Detected background noise photons per bit time:

$n_b := 10^6 \cdot \tau$ (assuming 10^6/sec)

$n_b = 0.02$

PMT PARAMETERS

Dark count per bit time: $n_d := 6.3 \cdot 10^4 \cdot \tau$

$n_d = 0.00126$

CALCULATION OF THE NOISE VARIANCES

Shot noise due to the signal:

$$N_s(n_s) := \left[m_{PN} \cdot n_s + \frac{2 \cdot N}{N+1} \cdot (1 - m_{PN}) \cdot n_s \right]$$

$$N_s(0.1) = 0.18991$$

Shot noise due to background light:

$$N_b := \frac{2 \cdot N}{N+1} \cdot n_b \qquad N_b = 0.03998$$

Shot noise due to dark counts:

$$N_d := \frac{2 \cdot N}{N+1} \cdot n_d \qquad N_d = 0.00252$$

CORRELATOR OUTPUT SNR:

$$SNR(n_s) := \frac{\sqrt{\frac{M \cdot (N+1)}{2}} \cdot m_{PN} \cdot n_s}{\sqrt{N_s(n_s) + N_b + N_d}} \qquad SNR(0.1) = 32.80153$$

Considering the loss due to misalignment between the histogrammer and the received PN code:

$$SNR_1(n_s) := \frac{1}{2} \cdot SNR(n_s)$$

CALCULATION OF RANGING ERROR PROBABILITY:

$$PE(n_s) := \frac{N-1}{2 \cdot \sqrt{\pi}} \cdot \int_{-20}^{20} \exp(-y^2) \cdot \left(1 - \operatorname{erf}\left(y + \frac{SNR_1(n_s)}{\sqrt{2}} \right) \right) dy$$

$TOL := 10^{-15}$ The integration error tolerance

NUMERICAL RESULTS

n_s	$\frac{n_s}{\tau}\cdot\frac{1}{10^6}$	$SNR_1(n_s)$	$20\cdot\log(SNR_1(n_s))$	$PE(n_s)$
0.02	1	5.57409	14.92349	0.08284
0.0225	1.125	6.09369	15.69761	0.01678
0.025	1.25	6.58971	16.37733	0.00324
0.0275	1.375	7.06469	16.98186	$6.00365\cdot10^{-4}$
0.03	1.5	7.52076	17.52523	$1.07339\cdot10^{-4}$
0.0325	1.625	7.95975	18.01798	$1.86082\cdot10^{-5}$
0.035	1.75	8.38321	18.46821	$3.14033\cdot10^{-6}$
0.0375	1.875	8.79251	18.88226	$5.17607\cdot10^{-7}$
0.04	2	9.18881	19.26519	$8.35592\cdot10^{-8}$
0.0425	2.125	9.57316	19.62111	$1.32431\cdot10^{-8}$
0.045	2.25	9.94646	19.95337	$2.06474\cdot10^{-9}$
0.0475	2.375	10.30953	20.26477	$3.17234\cdot10^{-10}$
0.05	2.5	10.66307	20.55764	$4.81053\cdot10^{-11}$

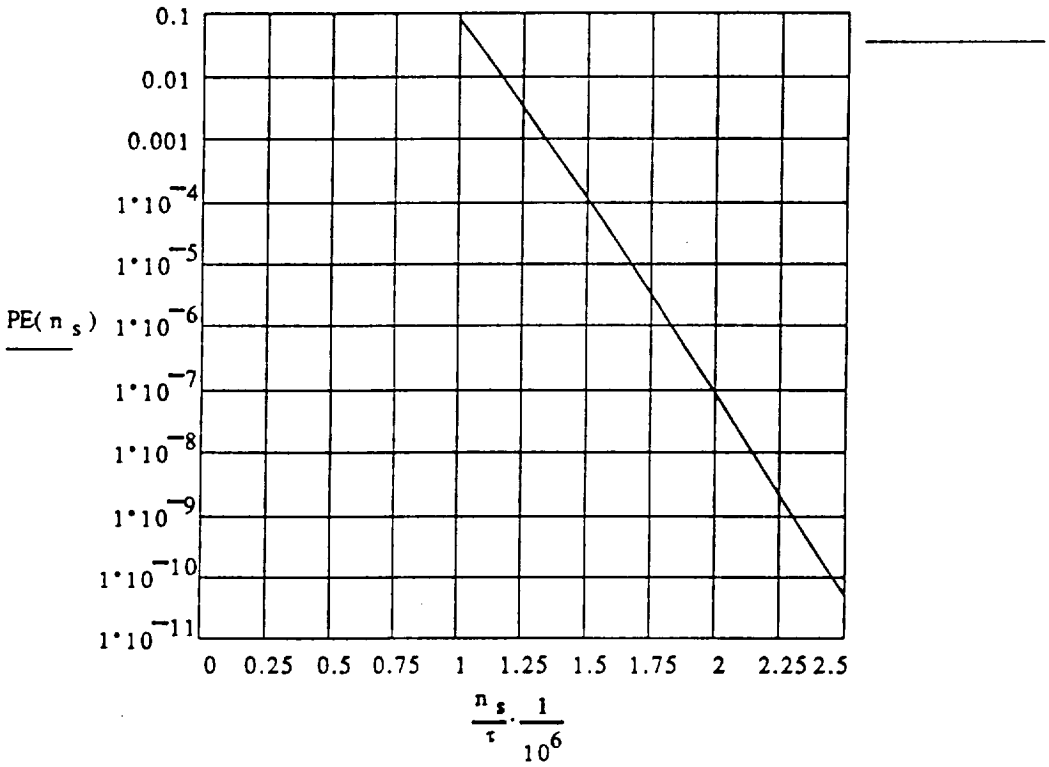

WRITEPRN(nsdat) $:= \frac{n_s}{\tau\cdot10^6}$ WRITEPRN(pevsns) $:= PE(n_s)$

GAMES PN Code Coarse Ranging Subsystem Performance

PN CODE PARAMETERS

Code Length: $N := 2047$

Code bit rate (bps): $BR := 50 \cdot 10^6$

Bit time (second): $\tau := \frac{1}{BR}$ $\tau = 2 \cdot 10^{-8}$

Total Integration time of the histogrammer (second): $T := 0.1$

Number of code length averaged:

$$M := \text{floor}\left(\frac{T}{\tau \cdot N}\right) \qquad M = 2.442 \cdot 10^3$$

DETECTED SIGNAL AND NOISE PHOTONS

Detected signal photons per bit time:

$$n_s := 0.05, 0.06 .. 0.2$$

Laser modulation index: $m_{PN} := 0.050$

Detected background noise photons per bit time:

$n_b := 10^6 \cdot \tau$ (assuming 10^6/sec)

$n_b = 0.02$

PMT PARAMETERS

Dark count per bit time: $n_d := 6.3 \cdot 10^4 \cdot \tau$

$n_d = 0.00126$

CALCULATION OF THE NOISE VARIANCES

Shot noise due to the signal:

$$N_s(n_s) := \left[m_{PN} \cdot n_s + \frac{2 \cdot N}{N+1} \cdot (1 - m_{PN}) \cdot n_s \right]$$

$$N_s(0.1) = 0.19491$$

Shot noise due to background light:

$$N_b := \frac{2 \cdot N}{N+1} \cdot n_b \qquad N_b = 0.03998$$

Shot noise due to dark counts:

$$N_d := \frac{2 \cdot N}{N+1} \cdot n_d \qquad N_d = 0.00252$$

CORRELATOR OUTPUT SNR:

$$SNR(n_s) := \frac{\sqrt{\frac{M \cdot (N+1)}{2}} \cdot m_{PN} \cdot n_s}{\sqrt{N_s(n_s) + N_b + N_d}} \qquad SNR(0.1) = 16.22731$$

Considering the loss due to misalignment between the histogrammer and the received PN code:

$$SNR_1(n_s) := \frac{1}{2} \cdot SNR(n_s)$$

CALCULATION OF RANGING ERROR PROBABILITY:

$$PE(n_s) := \frac{N-1}{2 \cdot \sqrt{\pi}} \cdot \int_{-20}^{20} \exp(-y^2) \cdot \left(1 - \operatorname{erf}\left(y + \frac{SNR_1(n_s)}{\sqrt{2}} \right) \right) dy$$

$TOL := 10^{-15}$ The integration error tolerance

NUMERICAL RESULTS

n_s	$\frac{n_s}{\tau}\cdot\frac{1}{10^6}$	$SNR_1(n_s)$	$20\cdot\log(SNR_1(n_s))$	$PE(n_s)$
0.05	2.5	5.28375	14.45884	0.19114
0.06	3	5.94033	15.47621	0.02725
0.07	3.5	6.54205	16.31428	0.00381
0.08	4	7.09994	17.02509	$5.27459\cdot10^{-4}$
0.09	4.5	7.62186	17.64122	$7.22913\cdot10^{-5}$
0.1	5	8.11366	18.18433	$9.84565\cdot10^{-6}$
0.11	5.5	8.57977	18.66952	$1.33472\cdot10^{-6}$
0.12	6	9.0237	19.10769	$1.80314\cdot10^{-7}$
0.13	6.5	9.44821	19.50699	$2.42957\cdot10^{-8}$
0.14	7	9.85556	19.87362	$3.26706\cdot10^{-9}$
0.15	7.5	10.24761	20.21245	$4.38643\cdot10^{-10}$
0.16	8	10.62591	20.52732	$5.88226\cdot10^{-11}$
0.17	8.5	10.99178	20.82136	$7.88051\cdot10^{-12}$
0.18	9	11.34633	21.09711	$1.05519\cdot10^{-12}$
0.19	9.5	11.69054	21.35669	$1.62124\cdot10^{-13}$
0.2	10	12.02523	21.60187	$1.91544\cdot10^{-14}$

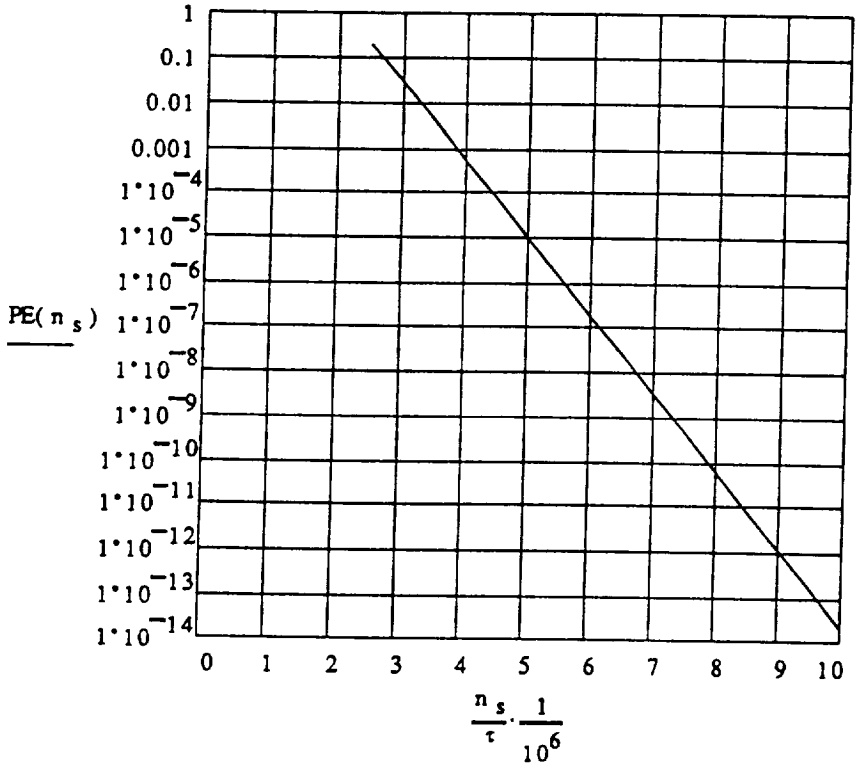

WRITEPRN(nsdat) := $\frac{n_s}{\tau\cdot10^6}$ WRITEPRN(pevsns) := $PE(n_s)$

Probability of Ranging Error vs Detected Signal Photons per Bit

PN CODE PARAMETERS

Code Length: $N := 127$

Code bit rate (bps): $BR := 1.5 \cdot 10^{6}$

Bit time (second): $\tau := \frac{1}{BR}$ $\tau = 6.66667 \cdot 10^{-7}$

Total Integration time of the histogrammer (second): $T := 0.1$

Number of code length averaged:

$$M := \text{floor}\left(\frac{T}{\tau \cdot N}\right) \qquad M = 1.181 \cdot 10^{3}$$

DETECTED SIGNAL AND NOISE PHOTONS

Detected signal photons per bit time:

$n_s := 1, 1.25 .. 3$

Laser modulation index: $m_{PN} := 0.85$

Detected background noise photons per bit time:

$n_b := 10$

APD PARAMETERS

APD Gain: $G := 200$

APD ionization coefficient ratio: $k_{eff} := 0.02$

APD excess noise factor: $F := k_{eff} \cdot G + \left(2 - \frac{1}{G}\right) \cdot (1 - k_{eff})$

$F = 5.9551$

APD bulk leakage current (A): $I_{db} := 1.0 \cdot 10^{-12}$

APD surface leakage current (A): $I_{ds} := 15 \cdot 10^{-9}$

PREAMPLIFIER NOISE

Preamplifier spectral noise current density (A^2/Hz):
(Analog Model 311 precision low noise current amplifiers)

$$N_{iamp} := (1.0 \cdot 10^{-12})^{2}$$

CALCULATION OF THE NOISE VARIANCES

Shot noise due to the signal:

$$N_s(n_s) := F\cdot\left[m_{PN}\cdot n_s + \frac{2\cdot N}{N+1}\cdot(1-m_{PN})\cdot n_s\right]$$

$N_s(10) = 68.34408$

Shot noise due to background light:

$$N_b := F\cdot\frac{2\cdot N}{N+1}\cdot n_b \qquad N_b = 118.17152$$

APD dark current noise:

Electron charge (C): $q := 1.6\cdot 10^{-19}$

$$N_d := \frac{2\cdot N}{N+1}\cdot\left(F\cdot\frac{I_{db}\cdot\tau}{q} + \frac{I_{ds}\cdot\tau}{q\,G^2}\right) \qquad N_d = 52.33872$$

Preamplifier noise:

$$N_a := \frac{2\cdot N}{N+1}\cdot\frac{N_{iamp}}{2\cdot G^2\cdot q^2}\cdot\tau \qquad N_a = 645.9554$$

CORRELATOR OUTPUT SNR:

$$SNR(n_s) := \frac{\sqrt{\frac{M\cdot(N+1)}{2}}\cdot m_{PN}\cdot n_s}{\sqrt{N_s(n_s)+N_b+N_d+N_a}}$$

condering the loss due to misalignment of the histogramer

$$SNR_1(n_s) := \frac{1}{2}\cdot SNR(n_s)$$

CALCULATION OF RANGING ERROR PROBABILITY:

$$PE(n_s) := \frac{N-1}{2\cdot\sqrt{\pi}}\cdot\int_{-20}^{20}\exp(-y^2)\cdot\left(1-\operatorname{erf}\left(y+\frac{SNR_1(n_s)}{\sqrt{2}}\right)\right)^{\cdot} dy$$

$TOL := 10^{-15}$ The integration error tolerance

NUMERICAL RESULTS

n_s	$SNR_1(n_s)$	$20 \cdot \log(SNR_1(n_s))$	$PE(n_s)$
1	4.07216	12.1965	0.25097
1.25	5.08493	14.12569	0.02039
1.5	6.0956	15.70033	0.00103
1.75	7.1042	17.0303	$3.19772 \cdot 10^{-5}$
2	8.11072	18.18119	$6.13791 \cdot 10^{-7}$
2.25	9.11519	19.19531	$7.26306 \cdot 10^{-9}$
2.5	10.1176	20.10155	$5.30124 \cdot 10^{-11}$
2.75	11.11797	20.92051	$2.38925 \cdot 10^{-13}$
3	12.11631	21.66741	0

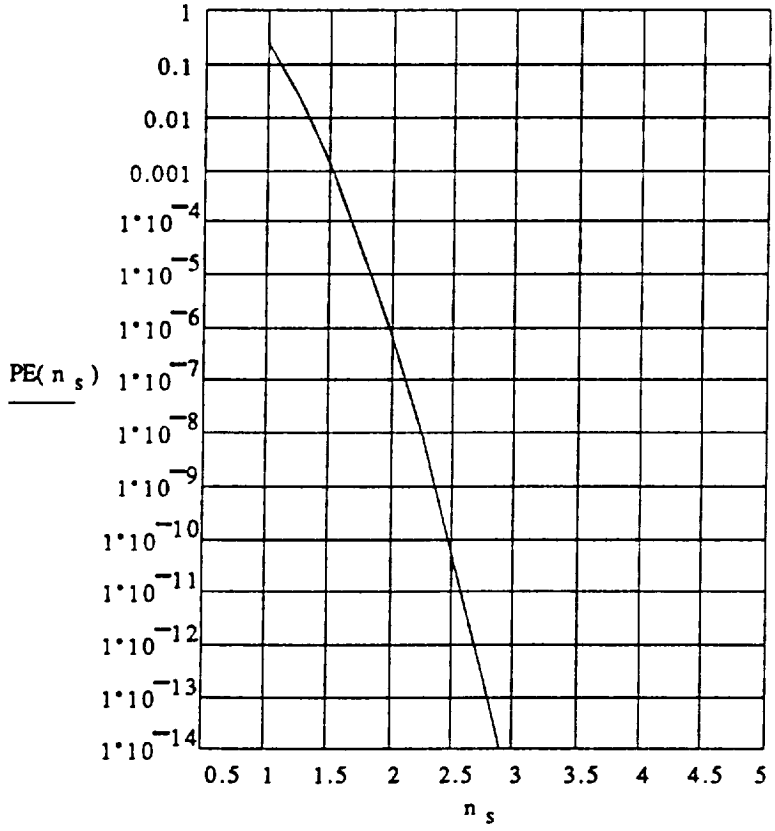

WRITEPRN(nsdat) := n_s

WRITEPRN(pevsns) := $PE(n_s)$

Power Spectrum of PN Ranging Codes

Xiaoli Sun/JHU, (Rev. 1) April 1994

A PN code sequence used in a ranging instrument can be written as

$$x(t)=\sum_{k=-\infty}^{\infty} a_k p(t-k\Delta t) \tag{1}$$

where $a_k = \pm 1$ is the value of the k^{th} bit of the PN code sequence, $p(t)$ is the pulse shape, and Δt is the bit interval. Here we assumed that the PN code is M bits long and repetitive.

The power spectrum of PN code sequence is given by [1, p. 35]

$$S(\omega)=\int_{-\infty}^{\infty} R(\tau)e^{-j\omega\tau}d\tau \tag{2}$$

where $R(\tau)$ is the autocorrelation function of the PN code defined as

$$R(\tau)=\frac{1}{T}\int_{-T/2}^{T/2} x(t)x(t+\tau)dt \tag{3}$$

1. Power Spectrum of Maximum PN Ranging Codes

When a maximum PN code [2] is used, the autocorrelation function can be written as

$$R_M(\tau)=\frac{M+1}{M}\sum_{n=1}^{\infty} \rho(\tau-nT)-\frac{1}{M} \tag{4}$$

where

$$\rho(\tau)=\frac{1}{\Delta t}\int_{-\infty}^{\infty} p(t)p(t+\tau)dt \tag{5}$$

Substituting (4) and (5) into (2)

$$S(\omega)=\frac{M+1}{M\Delta t}|P(\omega)|^2\sum_{n=-\infty}^{\infty} e^{-j n\omega T}-\frac{2\pi}{M}\delta(\omega) \tag{6}$$

where $P(\omega)$ is the Fourier transform of the pulse shape, i.e.,

$$|P(\omega)|^2=\int_{-\infty}^{\infty} p(\tau)e^{-j\omega\tau}d\tau=\left|\int_{-\infty}^{\infty} p(t)e^{-j\omega t}dt\right|^2 \tag{7}$$

Since [3]

$$\sum_{n=-\infty}^{\infty} e^{-jn\omega T} = \int_{-\infty}^{\infty}\left[\sum_{n=-\infty}^{\infty}\delta(t-nT)\right]e^{-j\omega t}dt = \frac{2\pi}{T}\sum_{n=-\infty}^{\infty}\delta(\omega- n\frac{2\pi}{T}) \tag{8}$$

the power spectrum of a maximum PN code, Eq. (6), becomes

$$S(\omega)=\frac{2\pi(M+1)}{M^2\Delta t^2}|P(\omega)|^2\sum_{n=-\infty}^{\infty}\delta(\omega- n\frac{2\pi}{T}) - \frac{2\pi}{M}\delta(\omega) \tag{9}$$

Therefore, the power spectrum of a maximum PN code consists of a series of discrete components at multiples of the repetition frequency of the PN sequence. The envelop of the spectrum is equal to the power spectrum of the pulse shape, $|P(\omega)|^2$.

2. Power Spectrum of JPL Ranging Code

The JPL ranging code [4] is formed by modulo 2 sum of several shorter binary code sequences called components. It has the advantage of fast target acquisition.

Let us first consider a JPL code, $Z=\{z_0, z_1,...,z_M\}$, which has two component code sequences, $X=\{x_0, x_1,...,x_{M1}\}$ and $Y=\{y_0, y_1,...,y_{M2}\}$, i.e., $Z=X\oplus Y$. Here x_i, y_i, and z_i are binary variables and equal to either 1 or zero. The length of the combined code is $M=M1\cdot M2$ where M1 and M2 have to be relative prime numbers.

The autocorrelation function of the binary sequence Z is given as

$$R_Z(n)=\frac{1}{M}\sum_{i=0}^{M-1} z_i \oplus z_{i+n}=\frac{1}{M1\times M2}\sum_{i1=0}^{M1-1}\sum_{i2=0}^{M2-1}(x_{i1}\oplus y_{i2})\oplus(x_{i1+n}\oplus y_{i2+n})$$

$$=\frac{1}{M1\times M2}\sum_{i1=0}^{M1-1}\sum_{i2=0}^{M2-1}(x_{i1}\ominus x_{i1+n})\oplus(y_{i2}\oplus y_{i2+n}) \qquad (10)$$

Eq. (10) may also be interpreted as the difference in the probabilities of "1" and "0" for the binary variable $z_i \ominus z_{i+n}$, or, equivalently, $(x_{1i}\oplus x_{i1+n})\oplus(y_{12}\ominus x_{i2+n})$, as,

$$R_Z(n)=p(0)-p(1) \qquad (11)$$

Similar to the example given in [1, p. 75, Figure 5.8], a Karnaugh chart can be used to help to calculate those probabilities.

$(x_{1i}\oplus x_{i1+n})\oplus(y_{12}\ominus x_{i2+n})$		y_{i2}, y_{i2-n}			
		00	01	11	10
x_{i1}, x_{i1+n}	00	0	1	0	1
	01	1	0	1	0
	11	0	1	0	1
	10	1	0	1	0

The binary sequence X and Y can be considered as statistically independent, i.e., $p(x_{i1},x_{i1+n},y_{i2},y_{i2+n})=p(x_{i1},x_{i1+n})\cdot p(y_{i2},y_{i2+n})$. For two relatively long component codes, the probability for (x_{i1}, x_{i1+n}) or (y_{i2}, y_{i2-n}) to have each of the four combinations are approximately equal and so is the probabilities of each outcome of the binary variable $(x_{1i}\oplus x_{i1+n})\ominus(y_{12}\oplus x_{i2+n})$.

When n is a multiple of the code length of either, but not both, component, two of the columns or rows of the above karnaugh chart are deleted. Nevertheless, the probabilities of each outcome for $(x_{1i} \oplus x_{i1+n}) \ominus (y_{12} \oplus x_{i2+n})$ are still approximately equal. When n is a multiple of both component code lengths, the value of $(x_{1i} \oplus x_{i1+n}) \ominus (y_{12} \oplus x_{i2+n})$ is always unity.

Therefore, the autocorrelation function of the JPL ranging code sequences can be approximated as

$$R_Z(n) \approx \begin{cases} 1, & n=0,\pm M,... \\ 0, & \text{otherwise} \end{cases} \qquad (12)$$

The error caused by the approximation decreases as the component code lengths increase.

The above result also applies to JPL code of arbitrary number of components. One can consider any one component and the combined sequence of the rest components as the two components. The two code lengths are still relative prime and each codes still consists of approximately equal numbers of 0's and 1's.

Since the autocorrelation function of a JPL ranging code is the same as that of a regular maximum PN code, their power spectrums must be the same.

It is the crosscorrelation functions in which JPL ranging codes differ from regular maximum PN ranging code.

References

[1] S. W. Golomb, editor, *Digital Communications with Space Applications*, Prentice-Hall, Englewood Cliffs, NJ, 1964.

[2] R. C. Dixon, *Spread Spectrum Systems*, 2nd Ed., John Wiley & Sons, New York, 1984, ch. 3.

[3] A. V. Oppenheim and A. S. Willsky, *Signals and Systems*, Prentice-Hall, Englewood Cliffs, New Jersey, 1983, p. 201.

[4] R. C. Titsworth, "Optimal Ranging Codes," *IEEE Trans. Space Electronics and Telemetry*, Vol. ??, pp. 19-30, March 1964.